



MAX-PLANCK-GESELLSCHAFT

**Max Planck Institute Magdeburg
Preprints**

Peter Benner

Hamdullah Yücel

**Adaptive Symmetric Interior Penalty
Galerkin method for boundary control
problems**



MAX-PLANCK-INSTITUT
FÜR DYNAMIK KOMPLEXER
TECHNISCHER SYSTEME
MAGDEBURG

Abstract

We investigate an a posteriori error analysis of adaptive finite element approximations of linear-quadratic boundary optimal control problems under bilateral bound constraints, which act on a Neumann boundary condition. We use a symmetric interior penalty Galerkin (SIPG) method as discretization method. An efficient and reliable residual-type error estimator is introduced by invoking data oscillations. We then derive local upper and lower a posteriori error estimates for the boundary control problem. Adaptive mesh refinement indicated by a posteriori error estimates is applied. Numerical results are presented to illustrate the performance of the adaptive finite element approximation.

Impressum:

Max Planck Institute for Dynamics of Complex Technical Systems, Magdeburg

Publisher:

Max Planck Institute for
Dynamics of Complex Technical Systems

Address:

Max Planck Institute for
Dynamics of Complex Technical Systems
Sandtorstr. 1
39106 Magdeburg

www.mpi-magdeburg.mpg.de/preprints

1 Introduction

Many real-life applications such as the shape optimization of technological devices [35], the identification of parameters in environmental processes, and flow control problems [11, 14, 37] lead to optimization problems governed by partial differential equations (PDEs). The complexity of such problems requires special care in order to obtain efficient numerical approximations for the optimization problem. One particular method is the adaptive finite element method, which consists of successive loops of the following sequence:

$$\mathbf{SOLVE} \rightarrow \mathbf{ESTIMATE} \rightarrow \mathbf{MARK} \rightarrow \mathbf{REFINE}. \quad (1)$$

The **SOLVE** step stands for the numerical solution of the optimization problem in a finite dimensional space defined on the given mesh. The **ESTIMATE** step is the key point of the adaptive finite element method. In this step, local error indicators are computed in terms of the discrete solutions without knowledge of the exact solutions. They are essential in designing algorithms for mesh adaptation, which equidistribute the computational effort and optimize the computation. Based on the information of the indicators, the **MARK** step selects a subset of elements subject to refinement. The refinement is then executed in the final step **REFINE** of the adaptive loop.

Adaptive mesh refinement is particularly attractive for the solution of optimal control problems, which exhibit layers or singularities in certain regions of the mesh. In this case, adaptivity allows local mesh refinement around the layers as needed, thereby achieving a desired residual bound with as few of degrees of freedom as possible. The vast majority of the literature about the a posteriori error analysis of optimal control problems is for distributed optimal control problems. We would like to mention the residual-type estimators [19, 21, 24, 30, 41, 42, 44, 45], and the goal oriented dual weighted approach [5, 16, 18, 40].

However, there exists limited work for the numerical solution of boundary optimal control problems. The residual-type error estimators are studied in [15, 22, 28, 33, 34], whereas the hierarchical-type estimators are studied in [28]. They all use continuous finite element discretizations. The results in [29] show that discontinuous Galerkin (DG) methods enjoy a better convergence behaviour for optimal control problems exhibiting boundary layers. Optimal convergence orders are obtained if the error is computed away from boundary or interior layers. Discontinuous Galerkin methods have several advantages over other types of finite element methods. For example, the state and test spaces are very easy to construct; they can naturally handle inhomogeneous boundary conditions and curved boundaries; and they have flexibility in handling non-matching grids and in designing hp-adaptive grid refinement. Though these methods are known since the 1970s, much attention has been paid only in the past few years due to the availability of cheap computing resources. We would like to refer to [3, 17, 23, 27, 25, 38] for details about discontinuous Galerkin methods. Discontinuous Galerkin methods have been studied in [29, 42, 43, 44, 45] for distributed optimal control problems. To the best of our knowledge, there exists no work for boundary optimal control problems with discontinuous Galerkin discretization.

In this paper, we derive reliable and efficient a posteriori error estimators for the boundary optimal control problems governed by elliptic equations, discretized by the symmetric interior penalty Galerkin (SIPG) method. We choose the SIPG as a discontinuous Galerkin method due to its symmetric property. This implies that discretization and optimization commute,

see, e.g., [43]. The a posteriori error analysis of the boundary control problem includes the error in state, adjoint, control, and co-control and also takes data oscillations into account, in order to consider the data of the problem (coefficients of the equations, right-hand side, boundary conditions) in the most general setting as possible. We note that data oscillations are also taken into consideration in [2, 36] for single state equations, and in [22, 24] for optimal control problems.

The remainder of the paper is organized as follows: In the next section, we introduce the Neumann boundary optimal control problem governed by a second order elliptic PDE with bilateral constraints on the control. The optimality conditions are given in terms of the state, the adjoint, the control and the co-control corresponding to the Lagrangian multiplier for the control. Section 3 describes the SIPG discretization of the boundary optimal control problem. A posteriori error estimators are given in Section 4. We use a residual-type error estimator for the global discretization errors in all variables which consists of edge and element residuals. The data oscillations are also used in the error analysis. We further derive local upper and lower a posteriori error estimates for the boundary control problem. Finally, in the last section, the adaptive cycle is described and numerical results are presented to illustrate the performance of our adaptive mesh refinement strategy.

2 The boundary control problem

We assume Ω to be an open, bounded polygonal domain in \mathbb{R}^2 with boundary $\Gamma = \overline{\Gamma_D} \cup \overline{\Gamma_N}$, $\Gamma_D \cap \Gamma_N = \emptyset$. We adopt standard notation from Lebesgue and Sobolev space theory (see, e.g., [1]) and refer to $(\cdot, \cdot)_{k,S}$ and $|\cdot|_{k,S}$, $\|\cdot\|_{k,S}$, $k \in \mathbb{N}$, $S \subseteq \Omega$, as the $H^k(S)$ -inner product and associated semi-norm and norm, respectively. In addition, c or C denotes a general positive constant.

We here consider the following boundary control problem governed by linear-quadratic elliptic equations with constrained controls on the part of the Neumann boundary

$$\underset{u \in U^{ad}}{\text{minimize}} \quad \frac{1}{2} \|y(x) - y^d(x)\|_{0,\Omega}^2 + \frac{\omega}{2} \|u(x) - u^d(x)\|_{0,\Gamma_N}^2 \quad (2)$$

subject to

$$-\Delta y(x) + \alpha(x)y(x) = f(x) \quad x \in \Omega, \quad (3a)$$

$$y(x) = g^D \quad x \in \Gamma_D, \quad (3b)$$

$$\frac{\partial y}{\partial n}(x) = u(x) + g^N \quad x \in \Gamma_N, \quad (3c)$$

with control constraints on a closed convex set U^{ad} given by

$$U^{ad} := \{v \in L^2(\Gamma_N) : u^a \leq v(x) \leq u^b \text{ a.e. } x \in \Gamma_N\}, \quad (4)$$

where $u^a, u^b \in L^\infty(\Gamma_N)$, with $u^a \leq u^b$ for almost all $x \in \Gamma_N$. The function u_d , called desired control, is a guideline for the control, see, e.g., [10, 19]. Note that this formulation also allows for the special and most common case $u_d = 0$, i.e., there is no a priori information on the optimal control.

We make the following assumptions on the functions and parameters in the optimal control problem (2)-(3) to show the well-posedness of the optimal control problem:

$$f, y^d \in L^2(\Omega), \quad u^d \in L^2(\Gamma_N), \quad g^D \in H^{1/2}(\Gamma_D), \quad g^N \in L^2(\Gamma_N), \quad \omega \in \mathbb{R}_+, \quad \alpha \in L^\infty(\Omega). \quad (5)$$

Let us first consider the weak formulation of the state equation (3). If we define the spaces of state and test functions by

$$Y = \{y \in H^1(\Omega) : y|_{\Gamma_D} = g^D\}, \quad V = \{v \in H^1(\Omega) : v|_{\Gamma_D} = 0\}$$

and the bilinear form by

$$a(y, v) = \int_{\Omega} (\nabla y \cdot \nabla v + \alpha y v) \, dx,$$

then the weak form of the state equation (3) for a fixed u reads as follows: find $y \in Y$ such that

$$a(y, v) = (f, v)_{0, \Omega} + (u + g^N, v)_{0, \Gamma_N} \quad \forall v \in V. \quad (6)$$

It is well-known that under the above assumptions (5), the boundary control problem (2)-(3) admits a unique solution $(y, u) \in Y \times U^{ad}$, see, e.g., [13, 31, 33]. The solution (y, u) is characterized by the existence of an adjoint $p \in V$ such that

$$a(y, v) = (f, v)_{0, \Omega} + (u + g^N, v)_{0, \Gamma_N} \quad \forall v \in V, \quad (7a)$$

$$a(\Psi, p) = -(y - y^d, \Psi)_{0, \Omega} \quad \forall \Psi \in V, \quad (7b)$$

$$(\omega(u - u^d) - p, v - u)_{0, \Gamma_N} \geq 0 \quad \forall v \in U^{ad}. \quad (7c)$$

Note that the inequality (7c) can be equivalently stated by invoking a Lagrange multiplier corresponding to the inequality constraints $\sigma \in L^2(\Gamma_N)$:

$$\omega(u - u^d) - p - \sigma^a + \sigma^b = 0 \quad \text{a.e. in } \Gamma_N, \quad (8a)$$

$$(\sigma^a, u^a - u)_{0, \Gamma_N} = (\sigma^b, u - u^b)_{0, \Gamma_N} = 0 \quad \text{a.e. in } \Gamma_N, \quad (8b)$$

$$\sigma = \sigma^b - \sigma^a, \quad \sigma^a \geq 0, \quad \sigma^b \geq 0, \quad u^a \leq u \leq u^b \quad \text{a.e. in } \Gamma_N \quad (8c)$$

with

$$\sigma = \max\{0, \sigma + \gamma(u - u^b)\} + \min\{0, \sigma - \gamma(u^a - u)\} \quad \text{a.e. in } \Gamma_N, \quad (9)$$

where γ is any positive constant.

It is well known that (8) enjoys the Newton differentiability property [20], at least for $\gamma = \omega$. Therefore, a generalized (semi-smooth) Newton iteration can be applied. We can express the Newton iteration in terms of an active set strategy due to the structure of the nonsmooth part (9). For any Newton iteration step, the active sets are then determined by

$$\mathcal{A}_a = \{x \in \Gamma_N : \sigma - \gamma(u^a - u) < 0\}, \quad (10a)$$

$$\mathcal{A}_b = \{x \in \Gamma_N : \sigma + \gamma(u - u^b) > 0\}, \quad (10b)$$

and the inactive set is $I = \Gamma_N \setminus \{\mathcal{A}_a \cup \mathcal{A}_b\}$. Then, the complimentary conditions in (8) can be rewritten as

$$u(x) = u^a, \quad \sigma^b = 0, \quad \sigma \leq 0, \quad \text{a.e. on } \mathcal{A}_a, \quad (11a)$$

$$u(x) = u^b, \quad \sigma^a = 0, \quad \sigma \geq 0, \quad \text{a.e. on } \mathcal{A}_b, \quad (11b)$$

$$u^a < u(x) < u^b, \quad \sigma^a = \sigma^b = 0, \quad \sigma = 0, \quad \text{a.e. on } I. \quad (11c)$$

3 Symmetric interior penalty Galerkin (SIPG) method

We discretize our optimal control problem (2)-(3) using a discontinuous Galerkin method, namely, the symmetric interior penalty Galerkin (SIPG) discretization due to the symmetry property of its bilinear form, i.e., $a_h(y, v) = a_h(v, y)$, see e.g., [3].

We assume that the domain Ω is polygonal such that the boundary is exactly represented by boundaries of triangles. We denote $\{\mathcal{T}_h\}_h$ as a family of shape-regular simplicial triangulations of Ω . Each mesh \mathcal{T}_h consists of closed triangles such that $\overline{\Omega} = \bigcup_{K \in \mathcal{T}_h} \overline{K}$ holds. We assume that the mesh is regular in the following sense: for different triangles $K_i, K_j \in \mathcal{T}_h$, $i \neq j$, the intersection $K_i \cap K_j$ is either empty or a vertex or an edge, i.e., hanging nodes are not allowed. The diameter of an element K and the length of an edge E are denoted by h_K and h_E , respectively.

We split the set of all edges \mathcal{E}_h into the set \mathcal{E}_h^0 of interior edges, the set \mathcal{E}_h^D of Dirichlet boundary edges and the set \mathcal{E}_h^N of Neumann boundary edges so that $\mathcal{E}_h = \mathcal{E}_h^D \cup \mathcal{E}_h^0$ with $\mathcal{E}_h^B = \mathcal{E}_h^D \cup \mathcal{E}_h^N$. Let the edge E be a common edge for two elements K and K^e . For a piecewise continuous scalar function y , there are two traces of y along E , denoted by $y|_E$ from inside K and $y^e|_E$ from inside K^e . The jump and average of y across the edge E are defined by:

$$[[y]] = y|_E \mathbf{n}_K + y^e|_E \mathbf{n}_{K^e}, \quad \{\{y\}\} = \frac{1}{2}(y|_E + y^e|_E), \quad (12)$$

where \mathbf{n}_K (resp. \mathbf{n}_{K^e}) denotes the unit outward normal to ∂K (resp. ∂K^e).

Similarly, for a piecewise continuous vector field ∇y , the jump and average across an edge E are given by

$$[[\nabla y]] = \nabla y|_E \cdot \mathbf{n}_K + \nabla y^e|_E \cdot \mathbf{n}_{K^e}, \quad \{\{\nabla y\}\} = \frac{1}{2}(\nabla y|_E + \nabla y^e|_E). \quad (13)$$

For a boundary edge $E \in K \cap \Gamma$, we set $\{\{\nabla y\}\} = \nabla y$ and $[[y]] = y \mathbf{n}$, where \mathbf{n} is the outward normal unit vector on Γ .

Recall that in discontinuous Galerkin methods, the state and test spaces consist of piecewise discontinuous polynomials. That is, no continuity constraints are explicitly imposed on the state and test functions across the element interfaces. As a consequence, weak formulations must include jump terms across interfaces, and typically penalty terms are added to control the jump terms. Then, we define the spaces of test functions, the discrete states and controls by

$$V_h = Y_h = \{y \in L^2(\Omega) : y|_K \in \mathbb{P}^1(K) \quad \forall K \in \mathcal{T}_h\}, \quad (14a)$$

$$U_{h,N} = \{u \in L^2(\Gamma_N) : u|_E \in \mathbb{P}^1(E) \quad \forall E \in \mathcal{E}_h^N\}, \quad (14b)$$

respectively. $\mathbb{P}^1(K)$ (resp. $\mathbb{P}^1(E)$) is the set of linear polynomials in K (resp. on E). Note that the space Y_h of discrete states and the space of test functions V_h are identical due to the weak treatment of boundary conditions in DG methods. We then introduce the following (bi-)linear forms for $\forall v \in V_h$ according to

$$a_h(y, v) = \sum_{K \in \mathcal{T}_h} \int_K (\nabla y \cdot \nabla v + \alpha y v) dx - \sum_{E \in \mathcal{E}_h^0 \cup \mathcal{E}_h^D} \int_E \left(\{\{\nabla y\}\} \cdot \llbracket v \rrbracket + \{\{\nabla v\}\} \cdot \llbracket y \rrbracket \right) ds \\ + \sum_{E \in \mathcal{E}_h^0 \cup \mathcal{E}_h^D} \frac{\sigma_0}{h_E} \int_E \llbracket y \rrbracket \cdot \llbracket v \rrbracket ds, \quad (15a)$$

$$b_h(u, v) = \sum_{E \in \mathcal{E}_h^N} \int_E uv ds, \quad (15b)$$

$$l_h(v) = \sum_{K \in \mathcal{T}_h} \int_K f v dx + \sum_{E \in \mathcal{E}_h^D} \int_E g^D \left(\frac{\sigma_0}{h_E} \mathbf{n}_E \cdot \llbracket v \rrbracket - \{\{\nabla v\}\} \right) ds + \sum_{E \in \mathcal{E}_h^N} \int_E g^N v ds, \quad (15c)$$

where the parameter $\sigma_0 \in \mathbb{R}_0^+$ is called the penalty parameter, which should be sufficiently large to ensure the stability of the DG discretization; independent of the mesh size h [38, Sec. 2.7.1]. However, large penalty parameters decrease the jumps across element interfaces, which can affect the numerical approximation. Further, the DG approximation converges to the continuous Galerkin approximation as the penalty parameter goes to infinity (see, e.g., [8] for details).

The bilinear form $a_h(\cdot, \cdot)$ is consistent with the state equation (3) for a fixed given control u in the following sense: if y satisfies (3), then

$$a_h(y, v) = (f + u, v)_{0, \Omega} + \sum_{E \in \mathcal{E}_h^D} (y, \frac{\sigma_0}{h_E} \mathbf{n}_E \cdot \llbracket v \rrbracket - \{\{\nabla v\}\})_{0, E} \\ + \sum_{E \in \mathcal{E}_h^N} (\mathbf{n}_E \cdot \nabla y, v)_{0, E}, \quad \forall v \in V_h. \quad (16)$$

We then define the SIPG approximation y_h of the solution y of the state system (3) for a fixed given control $u_h = u$ such that

$$a_h(y_h, v) = l_h(v) + b_h(u_h, v) \quad \forall v \in V_h. \quad (17)$$

Thus, we have the following orthogonality relation:

$$a_h(y - y_h, v) = 0 \quad \forall v \in V_h. \quad (18)$$

We need the following trace and inverse inequalities, which will be used frequently in the a posteriori error analysis, see e.g., [7, 26],

$$|v|_{0, \partial S} \leq c_{tr} \|v\|_{1, S}, \quad \forall v \in H^1(S), \quad (19a)$$

$$|v|_{0, \partial S} \leq c_{tr} (h_K^{-1} \|v\|_{0, S}^2 + h_K \|\nabla v\|_{0, S}^2), \quad \forall v \in H^1(S), \quad (19b)$$

and

$$|v|_{j, S} \leq c_{inv} h_S^{i-j} |v|_{i, S}, \quad \forall v \in \mathbb{P}_k(S), \quad 0 \leq i \leq j \leq 2. \quad (20)$$

Note that the constants c_{tr} in (19) are different for both trace inequalities. To ease the notation, they are denoted by the same notation. We can now state the continuity and coercivity of the bilinear form $a_h(\cdot, \cdot)$ in the following lemma [27, Lemma 3.1]:

Lemma 3.1 For $a_h(\cdot, \cdot)$ as in (15a), it holds:

(i)

$$|a_h(y, v)| \leq 2 \|y\| \|v\|, \quad \forall y, v \in Y_h. \quad (21)$$

(ii) There exists a positive constant c_a such that

$$a_h(v, v) \geq c_a \|v\|^2, \quad \forall v \in V_h \quad (22)$$

with the following mesh-dependent energy norm

$$\begin{aligned} \|v\| := & \left(\sum_{K \in \mathcal{T}_h} (\|\nabla v_h\|_{0,K}^2 + \alpha \|v\|_{0,K}^2) \right. \\ & \left. + \sum_{E \in \mathcal{E}_h^0 \cup \mathcal{E}_h^D} (h_E \|\{\{\nabla v\}\}\|_{0,E}^2 + \frac{\sigma_0}{h_E} \|[[v_h]]\|_{0,E}^2) \right)^{1/2}. \end{aligned} \quad (23)$$

The proof of (i) is an application of the Cauchy-Schwarz inequality, while the proof of (ii) is obtained by applying the trace (19b) and inverse (20) inequalities.

In the a posteriori error analysis, we invoke data oscillations, since we do not assume any regularity of the data. Then, the data of the problem (coefficients of the equation, right-hand side, boundary conditions) are approximated by using the finite element ansatz functions on the underlying triangulation. Let

$$f_h, y_h^d, \alpha_h \in V_h, \quad u_h^d, g_h^N, u_h^a, u_h^b \in U_{h,N}$$

denote approximations to the right hand side f , the desired state y^d , the reaction term α , the desired control u^d , the Neumann g^N boundary condition, the lower bound u^a and the upper bound u^b , respectively. Similarly, the Dirichlet boundary condition is approximated by $g_h^D \in U_{h,D} = \{y \in L^2(\Gamma_D) : y|_E \in \mathbb{P}^1(E) \quad \forall E \in \mathcal{E}_h^D\}$.

Then, the SIPG discretization of the boundary control problem (2)-(3) is given as follows:

$$\text{minimize } J(y_h, u_h) := \frac{1}{2} \sum_{K \in \mathcal{T}_h} \|y_h - y_h^d\|_{0,K}^2 + \sum_{E \in \mathcal{E}_h^N} \frac{\omega}{2} \|u_h\|_{0,E}^2 \quad (24a)$$

$$\text{over } (y_h, u_h) \in Y_h \times U_h^{ad}, \quad (24b)$$

$$\text{subject to } a_h(y_h, v_h) = l_h(v_h) + b_h(u_h, v_h), \quad v_h \in V_h \quad (24c)$$

with the discrete constraint set for the boundary controls

$$U_h^{ad} = \{u_h \in U_{h,N} : u_h^a \leq u_h \leq u_h^b\}. \quad (24d)$$

The optimality conditions of the discretized optimization problem (24) involve the existence of a discrete $p_h \in V_h$ such that

$$a_h(y_h, v_h) = l_h(v_h) + b_h(u_h, v_h) \quad \forall v_h \in V_h, \quad (25a)$$

$$a_h(\Psi_h, p_h) = -(y_h - y_h^d, \Psi_h)_{0,\Omega} \quad \forall \Psi_h \in V_h, \quad (25b)$$

$$(\omega(u_h - u_h^d) - p_h, v_h - u_h)_{0,\Gamma_N} \geq 0 \quad \forall v_h \in U_h^{ad}. \quad (25c)$$

As in the continuous setting, the condition (25c) can be rewritten by invoking the discrete co-control $\sigma_h \in U_{h,N}$:

$$\omega(u_h - u_h^d) - p_h - \sigma_h^a + \sigma_h^b = 0 \quad (26a)$$

$$(\sigma_h^a, u_h^a - u_h)_{0,\Gamma_N} = (\sigma_h^b, u_h - u_h^b)_{0,\Gamma_N} = 0, \quad (26b)$$

$$\sigma_h = \sigma_h^b - \sigma_h^a, \quad \sigma_h^a \geq 0, \quad \sigma_h^b \geq 0, \quad u_h^a \leq u_h \leq u_h^b. \quad (26c)$$

with the discrete co-control

$$\sigma_h = \max\{0, \sigma_h + \gamma(u_h - u_h^b)\} + \min\{0, \sigma_h - \gamma(u_h^a - u_h)\}. \quad (27)$$

We then define the discrete active sets as

$$\mathcal{A}_{a,h} = \bigcup \{E \in \mathcal{E}_h^N \mid \sigma_h - \gamma(u_h^a - u_h) < 0\}, \quad (28a)$$

$$\mathcal{A}_{b,h} = \bigcup \{E \in \mathcal{E}_h^N \mid \sigma_h + \gamma(u_h - u_h^b) > 0\}, \quad (28b)$$

and the inactive set is $I_h = \mathcal{E}_h^N \setminus \{\mathcal{A}_{a,h} \cup \mathcal{A}_{b,h}\}$. Further, the complimentary conditions in (26) can be rewritten as in the continuous setting

$$u_h(x) = u_h^a, \quad \sigma_h^b = 0, \quad \sigma_h \leq 0, \quad \text{a.e. on } \mathcal{A}_{a,h}, \quad (29a)$$

$$u_h(x) = u_h^b, \quad \sigma_h^a = 0, \quad \sigma_h \geq 0, \quad \text{a.e. on } \mathcal{A}_{b,h}, \quad (29b)$$

$$u_h^a < u_h(x) < u_h^b, \quad \sigma_h^a = \sigma_h^b = 0, \quad \sigma_h = 0, \quad \text{a.e. on } I_h. \quad (29c)$$

4 The residual type a posteriori error estimator

We here introduce a residual-type error estimator for the optimal control problem (2)-(3), consisting of easily computable element and edge residuals with respect to the SIPG approximation. The error in the state y and adjoint p are measured by the energy norm $\|\cdot\|$, which is defined in (23), while the error in the control u and co-control σ are measured by the L^2 -norm on the Neumann boundary Γ_N .

The residual-type error estimator η for the SIPG approximation of the boundary control problem (2)-(3) is

$$\eta = \left(\eta_y^2 + \eta_p^2 + \eta_u^2 \right)^{1/2}, \quad (30)$$

where the state, the adjoint and the control estimators are defined according to

$$\eta_y = \left(\sum_{K \in \mathcal{T}_h} \eta_{y,K}^2 + \sum_{E \in \mathcal{E}_h^0} \eta_{y,E^0}^2 + \sum_{E \in \mathcal{E}_h^D} \eta_{y,E^D}^2 + \sum_{E \in \mathcal{E}_h^N} \eta_{y,E^N}^2 \right)^{1/2}, \quad (31a)$$

$$\eta_p = \left(\sum_{K \in \mathcal{T}_h} \eta_{p,K}^2 + \sum_{E \in \mathcal{E}_h^0} \eta_{p,E^0}^2 + \sum_{E \in \mathcal{E}_h^D} \eta_{p,E^D}^2 + \sum_{E \in \mathcal{E}_h^N} \eta_{p,E^N}^2 \right)^{1/2}, \quad (31b)$$

$$\eta_u = \left(\sum_{E \in \mathcal{E}_h^N} \eta_{u,E^N}^2 \right)^{1/2}, \quad (31c)$$

respectively. The element residuals $\eta_{y,K}, \eta_{p,K}$ are given by

$$\eta_{y,K} = h_K \|f_h + \Delta y_h - \alpha_h y_h\|_{0,K} \quad K \in \mathcal{T}_h, \quad (32a)$$

$$\eta_{p,K} = h_K \|-(y_h - y_h^d) + \Delta p_h - \alpha_h p_h\|_{0,K} \quad K \in \mathcal{T}_h. \quad (32b)$$

The edge residuals $\eta_{y,E^0}, \eta_{p,E^0}$ associated with the interior edges $E \in \mathcal{E}^0$ are

$$\eta_{y,E^0} = h_E^{1/2} \|[\![\nabla y_h]\!] \|_{0,E} + \sigma_0 h_E^{-1/2} \|[\![y_h]\!] \|_{0,E} \quad E \in \mathcal{E}_h^0 \quad (33a)$$

$$\eta_{p,E^0} = h_E^{1/2} \|[\![\nabla p_h]\!] \|_{0,E} + \sigma_0 h_E^{-1/2} \|[\![p_h]\!] \|_{0,E} \quad E \in \mathcal{E}_h^0, \quad (33b)$$

and the boundary edge residuals $\eta_{y,E^D}, \eta_{p,E^D}$ and $\eta_{y,E^N}, \eta_{p,E^N}, \eta_{u,E^N}$ with respect to the Dirichlet $E \in \mathcal{E}^D$ and Neumann boundary edges $E \in \mathcal{E}^N$ are

$$\eta_{y,E^D} = \sigma_0 h_E^{-1/2} \|g_h^D - y_h\|_{0,E} \quad \eta_{p,E^D} = \sigma_0 h_E^{-1/2} \|p_h\|_{0,E} \quad E \in \mathcal{E}_h^D, \quad (34a)$$

$$\eta_{y,E^N} = h_E^{1/2} \|u_h + g_h^N - \mathbf{n}_E \cdot \nabla y_h\|_{0,E} \quad \eta_{p,E^N} = h_E^{1/2} \|\mathbf{n}_E \cdot \nabla p_h\|_{0,E} \quad E \in \mathcal{E}_h^N, \quad (34b)$$

$$\eta_{u,E^N} = h_E \|\mathbf{n}_E \cdot \nabla (\omega(u_h - u_h^d) - p_h)\|_{0,E} \quad E \in \mathcal{E}_h^N. \quad (34c)$$

We further invoke data oscillations in the error analysis

$$\theta = (\theta_y^2 + \theta_p^2 + \theta_u^2)^{1/2}, \quad (35)$$

where

$$\theta_y^2 = \sum_{K \in \mathcal{T}_h} \underbrace{h_K^2 (\|f - f_h\|_{0,K}^2 + \|(\alpha - \alpha_h)y_h\|_{0,K}^2)}_{\theta_{y,K}^2} + \sum_{E \in \mathcal{E}_h^D} \underbrace{h_E^{-1} \|g^D - g_h^D\|_{0,E}^2}_{\theta_{y,E^D}^2} \quad (36a)$$

$$+ \sum_{E \in \mathcal{E}_h^N} \underbrace{h_E \|g^N - g_h^N\|_{0,E}^2}_{\theta_{y,E^N}^2},$$

$$\theta_p^2 = \sum_{K \in \mathcal{T}_h} \underbrace{h_K^2 (\|y^d - y_h^d\|_{0,K}^2 + \|(\alpha - \alpha_h)p_h\|_{0,K}^2)}_{\theta_{p,K}^2}, \quad (36b)$$

$$\theta_u^2 = \sum_{E \in \mathcal{E}_h^N} \underbrace{(\|\omega\| u^d - u_h^d\|_{0,E}^2 + \|u^a - u_h^a\|_{0,E}^2 + \|u^b - u_h^b\|_{0,E}^2)}_{\theta_{u,E^N}^2}. \quad (36c)$$

4.1 Reliability of the error estimator

In this section, we derive an upper bound for the discretization errors of the state, the adjoint, the control, and the co-control. The reliability means that up to data oscillations (35), the discretization errors can be bounded by the residual-type error estimator η (30).

To prove our reliability result, we need the auxiliary solutions $y[u_h], p[u_h] \in Y$, which solve the following system

$$a(y[u_h], v) = (f, v)_{0,\Omega} + (u_h + g^N, v)_{0,\Gamma_N} \quad \forall v \in V, \quad (37a)$$

$$a(q, p[u_h]) = -(y[u_h] - y^d, q)_{0,\Omega} \quad \forall q \in V. \quad (37b)$$

By (7) and (37), we obtain

$$a(y - y[u_h], v) = (u - u_h, v)_{0, \Gamma_N}, \quad \text{and} \quad a(q, p - p[u_h]) = (y[u_h] - y, q)_{0, \Omega}.$$

Then, by using Lemma 3.1 with the trace inequality (19a), we obtain the following relations

$$\|y - y[u_h]\| \leq c_{tr} c_0 c_a^{-1} \|u - u_h\|_{0, \Gamma_N}, \quad (38a)$$

$$\|p - p[u_h]\| \leq c_0 c_a^{-1} \|y - y[u_h]\|_{0, \Omega}, \quad (38b)$$

where $c_0 = \min(\alpha, \alpha^{-1})$.

We now find a bound, up to the control estimator η_u and the data oscillation θ_u , for the discretization errors in terms of the auxiliary state $y[u_h]$ and the auxiliary adjoint $p[u_h]$.

Lemma 4.1 *Let (y, p, u) and (y_h, p_h, u_h) be the solutions of (7) and (25), respectively, and let the co-control σ and the discrete co-control σ_h be defined in (8) and (26), respectively. Assume that $U_h^{ad} \subset U^{ad}$, $(\omega(u_h - u_h^d) - p_h)|_{E \in \mathcal{E}_h^N} \in H^1(E)$ and that there is a $v_h \in U_h^{ad}$ such that [33]*

$$\|(\omega(u_h - u_h^d) - p_h, v_h - u)\|_{0, \Gamma_N} \leq C \sum_{E \in \mathcal{E}_h^N} h_E \|\mathbf{n}_E \cdot \nabla(\omega(u_h - u_h^d) - p_h)\|_{0, E} \|u - u_h\|_{0, E}. \quad (39)$$

Then, there exist positive constants C_i , $1 \leq i \leq 4$, depending on the regularization parameter ω , the coercivity constant c_a and Ω , such that

$$\begin{aligned} \|u - u_h\|_{0, \Gamma_N} + \|\sigma - \sigma_h\|_{0, \Gamma_N} + \|y - y_h\| + \|p - p_h\| \\ \leq C_1 \eta_u + C_2 \theta_u + C_3 \|p[u_h] - p_h\| + C_4 \|y[u_h] - y_h\|. \end{aligned} \quad (40)$$

Proof. In view of (7), (25) and (38), we have

$$\|y - y_h\| \leq c_{tr} c_0 c_a^{-1} \|u - u_h\|_{0, \Gamma_N} + \|y[u_h] - y_h\|, \quad (41a)$$

$$\begin{aligned} \|p - p_h\| &\leq c_a^{-1} c_0 \|y - y[u_h]\|_{0, \Omega} + \|p[u_h] - p_h\| \\ &\leq c_a^{-1} c_0^2 \|y - y[u_h]\| + \|p[u_h] - p_h\|. \end{aligned} \quad (41b)$$

By the inequalities (26), (38) and an application of the trace inequality (19a), we find

$$\begin{aligned} \|\sigma - \sigma_h\|_{0, \Gamma_N} &= \omega \|u_h - u\|_{0, \Gamma_N} + \omega \|u^d - u_h^d\|_{0, \Gamma_N} + \|p - p_h\|_{0, \Gamma_N} \\ &\leq (\omega + c_{tr}^2 c_a^{-2} c_0^4) \|u_h - u\|_{0, \Gamma_N} + \omega \|u^d - u_h^d\|_{0, \Gamma_N} + c_{tr} c_0 \|p[u_h] - p_h\|. \end{aligned} \quad (42)$$

By the optimal equalities (7c) and (25c), we obtain

$$\begin{aligned} \omega \|u - u_h\|_{0, \Gamma_N}^2 &= (\omega u, u - u_h)_{0, \Gamma_N} - (\omega u_h, u - u_h)_{0, \Gamma_N} \\ &\leq (\omega u^d + p, u - u_h)_{0, \Gamma_N} - (\omega u_h, u - u_h)_{0, \Gamma_N} \\ &= -(\omega(u_h - u_h^d) - p_h, u - u_h)_{0, \Gamma_N} + (p - p_h, u - u_h)_{0, \Gamma_N} + \omega(u^d - u_h^d, u - u_h)_{0, \Gamma_N} \\ &\leq (\omega(u_h - u_h^d) - p_h, v_h - u)_{0, \Gamma_N} + (p - p_h, u - u_h)_{0, \Gamma_N} + \omega(u^d - u_h^d, u - u_h)_{0, \Gamma_N}. \end{aligned} \quad (43)$$

For the first term on the right-hand side of (43), in view of the assumption in (39), and an application of Young's inequality, we obtain

$$\begin{aligned} (\omega(u_h - u_h^d) - p_h, v_h - u)_{0,\Gamma_N} &\leq \frac{2}{\omega} \sum_{E \in \mathcal{E}_h^N} h_E^2 \|\mathbf{n} \cdot \nabla(\omega(u_h - u_h^d) - p_h)\|_{0,E}^2 \\ &\quad + \frac{\omega}{8} \|u - u_h\|_{0,\Gamma_N}^2. \end{aligned} \quad (44)$$

We split the second term on the right-hand side in (43) according to

$$(p - p_h, u - u_h)_{0,\Gamma_N} = (p - p[u_h], u - u_h)_{0,\Gamma_N} + (p[u_h] - p_h, u - u_h)_{0,\Gamma_N}. \quad (45)$$

The auxiliary equations in (37) yield

$$\begin{aligned} (u - u_h, p - p[u_h])_{0,\Gamma_N} &= (u, p - p[u_h])_{0,\Gamma_N} - (u_h, p - p[u_h])_{0,\Gamma_N}, \\ &= a(y - y[u_h], p) - a(y - y[u_h], p[u_h]), \\ &= (y - y[u_h], y[u_h] - y)_{0,\Omega} = -\|y - y[u_h]\|_{0,\Omega}^2 \leq 0. \end{aligned} \quad (46)$$

Using Young's inequality with the inequality (46) and the trace inequality (19a), we obtain

$$(p - p_h, u - u_h)_{0,\Gamma_N} \leq \frac{\omega}{4} \|u - u_h\|_{0,\Gamma_N}^2 + \frac{c_{tr}^2 c_0^2}{\omega} \|p[u_h] - p_h\|^2. \quad (47)$$

The last term on the right-hand side of (43) can be estimated by invoking Young's inequality again, such that

$$\omega(u^d - u_h^d, u - u_h)_{0,\Gamma_N} \leq \frac{\omega}{8} \|u - u_h\|_{0,\Gamma_N}^2 + \frac{2}{\omega} \|\omega(u^d - u_h^d)\|_{0,\Gamma_N}^2. \quad (48)$$

Then, using (44), (47)-(48), we end up with

$$\begin{aligned} \|u - u_h\|_{0,\Gamma_N}^2 &\leq \frac{2c_{tr}^2 c_0^2}{\omega^2} \|p[u_h] - p_h\|_{0,\Gamma_N}^2 + \frac{4}{\omega^2} \|\omega(u^d - u_h^d)\|_{0,\Gamma_N}^2 \\ &\quad + \frac{4}{\omega^2} \sum_{E \in \mathcal{E}_h^N} h_E^2 \|\mathbf{n} \cdot \nabla(\omega(u_h - u_h^d) - p_h)\|_{0,E}^2. \end{aligned} \quad (49)$$

Finally, combining (41), (42), and (49), the desired result is obtained. \square

It follows from Lemma 4.1 that we need to find a bound for $\|p[u_h] - p_h\|$. Now, we derive an upper bound for the errors between auxiliary solutions and discrete solutions in terms of the error estimators and data oscillations.

Lemma 4.2 *If $(y[u_h], p[u_h])$ and (y_h, p_h) are the solutions of (37) and (25), respectively, then*

$$\|p[u_h] - p_h\|^2 \leq C(\eta_p^2 + \theta_p^2 + \|y[u_h] - y_h\|_{0,\Omega}^2), \quad (50a)$$

$$\|y[u_h] - p_h\|^2 \leq C(\eta_y^2 + \theta_y^2). \quad (50b)$$

Proof. Let $e_p = p[u_h] - p_h$. By using the coercivity result (21) and the orthogonality relation (18), we obtain

$$\begin{aligned} c_a \|e_p\|^2 &\leq a_h(e_p, e_p) - a_h(v_h, e_p) = a_h(\Psi, e_p) \\ &= (y^d - y[u_h], \Psi)_{0,\Omega} - \left(\sum_{K \in \mathcal{T}_h} (\nabla \Psi, \nabla p_h)_{0,K} + \alpha(\Psi, p_h)_{0,K} \right) \\ &\quad + \sum_{E \in \mathcal{E}_h^0 \cup \mathcal{E}_h^D} \left[(\{\{\nabla \Psi\}\}, \llbracket p_h \rrbracket)_{0,E} + (\{\{\nabla p_h\}\}, \llbracket \Psi \rrbracket)_{0,E} - \frac{\sigma_0}{h_E} (\llbracket \Psi \rrbracket, \llbracket p_h \rrbracket)_{0,E} \right]. \end{aligned} \quad (51)$$

Integrating by parts, we see that

$$\begin{aligned} \sum_{K \in \mathcal{T}_h} (\nabla p_h, \nabla \Psi)_{0,K} &= \sum_{K \in \mathcal{T}_h} (-\Delta p_h, \Psi)_{0,K} + \sum_{E \in \mathcal{E}_h^0} \left[(\{\{\nabla p_h\}\}, \llbracket \Psi \rrbracket)_{0,E} + (\llbracket \nabla p_h \rrbracket, \{\{\Psi\}\})_{0,E} \right] \\ &\quad + \sum_{E \in \mathcal{E}_h^D} (\mathbf{n}_E \cdot \nabla p_h, \Psi)_{0,E} + \sum_{E \in \mathcal{E}_h^N} (\mathbf{n}_E \cdot \nabla p_h, \Psi)_{0,E}. \end{aligned} \quad (52)$$

Now, using (52) in (51) with the addition and subtraction of the given data, we obtain

$$\begin{aligned} c_a \|e_p\|^2 &\leq \sum_{K \in \mathcal{T}_h} \left[(y_h^d - y_h + \Delta p_h - \alpha_h p_h, \Psi)_{0,K} + (y^d - y_h^d, \Psi)_{0,K} + ((\alpha_h - \alpha) p_h, \Psi)_{0,K} \right] \\ &\quad + \sum_{K \in \mathcal{T}_h} (y_h - y[u_h], \Psi)_{0,K} + \sum_{E \in \mathcal{E}_h^D} (\mathbf{n}_E \cdot \nabla \Psi - \frac{\sigma_0}{h_E} \Psi, p_h) - \sum_{E \in \mathcal{E}_h^N} (\mathbf{n}_E \cdot \nabla p_h, \Psi)_{0,E} \\ &\quad + \sum_{E \in \mathcal{E}_h^0} \left[(\{\{\nabla \Psi\}\}, \llbracket p_h \rrbracket)_{0,E} - \frac{\sigma_0}{h_E} (\llbracket \Psi \rrbracket, \llbracket p_h \rrbracket)_{0,E} - (\llbracket \nabla p_h \rrbracket, \{\{\Psi\}\})_{0,E} \right]. \end{aligned} \quad (53)$$

For all $\zeta \in V_h \cap H^1(\Omega)$ with $\zeta|_{\Gamma_D} = 0$, the orthogonality relation (18) yields

$$\begin{aligned} 0 = a_h(e_p, p_h - \zeta) &= \sum_{K \in \mathcal{T}_h} (\nabla e_p, \nabla (p_h - \zeta))_{0,K} + \alpha(e_p, p_h - \zeta)_{0,K} \\ &\quad - \sum_{E \in \mathcal{E}_h^0} (\{\{\nabla (p_h - \zeta)\}\}, \llbracket e_p \rrbracket)_{0,E} - \sum_{E \in \mathcal{E}_h^D} (\mathbf{n}_E \cdot \nabla (p_h - \zeta), e_p)_{0,E} \\ &\quad - \sum_{E \in \mathcal{E}_h^0} (\{\{\nabla e_p\}\}, \llbracket p_h \rrbracket)_{0,E} - \sum_{E \in \mathcal{E}_h^D} (\mathbf{n}_E \cdot \nabla e_p, p_h)_{0,E} \\ &\quad + \sum_{E \in \mathcal{E}_h^0} \frac{\sigma_0}{h_E} (\llbracket e_p \rrbracket, \llbracket p_h \rrbracket)_{0,E} - \sum_{E \in \mathcal{E}_h^D} \frac{\sigma_0}{h_E} (p_h, p_h)_{0,E}. \end{aligned} \quad (54)$$

Letting $\Psi = e_p - v_h$, where v_h is piecewise constant on \mathcal{T}_h and using (54) in (53), we obtain

$$\begin{aligned} c_a \|e_p\|^2 &\leq \sum_{K \in \mathcal{T}_h} \left[(y_h^d - y_h + \Delta p_h - \alpha_h p_h, \Psi)_{0,K} + (y^d - y_h^d, \Psi)_{0,K} + ((\alpha_h - \alpha) p_h, \Psi)_{0,K} \right] \\ &\quad + \sum_{K \in \mathcal{T}_h} (y_h - y[u_h], \Psi)_{0,K} - \sum_{E \in \mathcal{E}_h^0} \left[\frac{\sigma_0}{h_E} (\llbracket p_h \rrbracket, \llbracket \Psi \rrbracket)_{0,E} + (\llbracket \nabla p_h \rrbracket, \{\{\Psi\}\})_{0,E} \right] \end{aligned}$$

$$\begin{aligned}
& - \sum_{E \in \mathcal{E}_h^D} \frac{\sigma_0}{h_E} (\boldsymbol{\Psi}, p_h)_{0,E} - \sum_{E \in \mathcal{E}_h^N} (\mathbf{n}_E \cdot \nabla p_h, \boldsymbol{\Psi})_{0,E} \\
& + \sum_{K \in \mathcal{T}_h} \left[(\nabla e_p, \nabla(p_h - \zeta))_{0,K} + \alpha(e_p, p_h - \zeta)_{0,K} \right] - \sum_{E \in \mathcal{E}_h^0} (\{\{\nabla(p_h - \zeta)\}\}, \llbracket e_p \rrbracket)_{0,E} \\
& - \sum_{E \in \mathcal{E}_h^D} (\mathbf{n}_E \cdot \nabla(p_h - \zeta), e_p)_{0,E} - \sum_{E \in \mathcal{E}_h^0} \frac{\sigma_0}{h_E} (\llbracket p_h \rrbracket, \llbracket p_h \rrbracket)_{0,E} - \sum_{E \in \mathcal{E}_h^D} \frac{\sigma_0}{h_E} (p_h, p_h)_{0,E}. \quad (55)
\end{aligned}$$

We now obtain bounds for the terms on the right-hand side of (55). The terms containing $\boldsymbol{\Psi}$ are bounded by

$$\begin{aligned}
& \frac{1}{\lambda_1} \left(h_K^2 \sum_{K \in \mathcal{T}_h} \|y_h^d - y_h + \Delta p_h - \alpha_h p_h\|_{0,K}^2 + \|y^d - y_h^d\|_{0,K}^2 + \|(\alpha_h - \alpha)p_h\|_{0,K}^2 \right) \quad (56) \\
& \frac{1}{\lambda_1} h_K^2 \sum_{K \in \mathcal{T}_h} \|y_h - y[u_h]\|_{0,K}^2 + \frac{1}{\lambda_2} \sum_{E \in \mathcal{E}_h^0} h_E \|\llbracket \nabla p_h \rrbracket\|_{0,E}^2 + \frac{1}{\lambda_3} \sum_{E \in \mathcal{E}_h^0} \sigma_0 h_E^{-1} \|\llbracket p_h \rrbracket\|_{0,E}^2 \\
& + \frac{1}{\lambda_4} \sum_{E \in \mathcal{E}_h^D} \sigma_0 h_E^{-1} \|p_h\|_{0,E}^2 + \frac{1}{\lambda_5} \sum_{E \in \mathcal{E}_h^N} h_E \|\mathbf{n} \cdot \nabla p_h\|_{0,E}^2 + \lambda_1 \sum_{K \in \mathcal{T}_h} h_K^{-2} \|\boldsymbol{\Psi}\|_{0,K}^2 \\
& + \lambda_2 \sum_{E \in \mathcal{E}_h^0} h_E^{-1} \|\{\{\nabla \boldsymbol{\Psi}\}\}\|_{0,E}^2 + \lambda_3 \sum_{E \in \mathcal{E}_h^0} \sigma_0 h_E^{-1} \|\llbracket \boldsymbol{\Psi} \rrbracket\|_{0,E}^2 + \lambda_4 \sum_{E \in \mathcal{E}_h^D} \sigma_0 h_E^{-1} \|\boldsymbol{\Psi}\|_{0,E}^2 \\
& + \lambda_5 \sum_{E \in \mathcal{E}_h^N} h_E^{-1} \|\boldsymbol{\Psi}\|_{0,E}^2
\end{aligned}$$

for any $\lambda_i > 0, i = 1, 2, 3, 4, 5$. To estimate the terms containing $\boldsymbol{\Psi}$ in (56), we choose v_h as the best piecewise constant approximation of e_p . Then, using an approximation result of [4]

$$\|\boldsymbol{\Psi}\|_{0,K} \leq ch_K \|\nabla e_p\|_{0,K} \quad K \in \mathcal{T}_h$$

with the trace inequality (19b), we obtain

$$\sum_{K \in \mathcal{T}_h} h_K^{-2} \|\boldsymbol{\Psi}\|_K^2 \leq c \sum_{K \in \mathcal{T}_h} \|\nabla e_p\|_K^2, \quad (57a)$$

$$\begin{aligned}
\sum_{E \in \mathcal{E}_h^0} h_E^{-1} (\|\{\{\nabla \boldsymbol{\Psi}\}\}\|_{0,E}^2 + \|\llbracket \boldsymbol{\Psi} \rrbracket\|_{0,E}^2) & \leq c \sum_{E \in \mathcal{E}_h^0} \sum_{K=K, K^e} h_E^{-1} (h_K^{-1} \|\boldsymbol{\Psi}\|_{0,K}^2 + h_K \|\mathbf{n}_E \cdot \nabla \boldsymbol{\Psi}\|_{0,K}^2) \\
& \leq c \sum_{K \in \mathcal{T}_h} \|\nabla e_p\|_K^2, \quad (57b)
\end{aligned}$$

$$\begin{aligned}
\sum_{E \in \mathcal{E}_h^D} h_E^{-1} \|\boldsymbol{\Psi}\|_{0,E}^2 & \leq c \sum_{E \in \mathcal{E}_h^0} \sum_{K=K} h_E^{-1} (h_K^{-1} \|\boldsymbol{\Psi}\|_{0,K}^2 + h_K \|\mathbf{n}_E \cdot \nabla \boldsymbol{\Psi}\|_{0,K}^2) \\
& \leq c \sum_{K \in \mathcal{T}_h} \|\nabla e_p\|_K^2. \quad (57c)
\end{aligned}$$

Note that here we use $h_E^{-1} h_K \leq 1$, which holds by the shape regularity of the mesh. The terms

containing $p_h - \zeta$ on the right-hand side of (55) are also bounded by

$$\begin{aligned}
& \lambda_8 \sum_{K \in \mathcal{T}_h} \|\nabla e_p\|_{0,K}^2 + \frac{1}{\lambda_8} \sum_{K \in \mathcal{T}_h} \|\nabla(p_h - \zeta)\|_{0,K}^2 + \lambda_9 \sum_{K \in \mathcal{T}_h} \alpha \|e_p\|_{0,K}^2 \\
& + \frac{1}{\lambda_9} \sum_{K \in \mathcal{T}_h} \|p_h - \zeta\|_{0,K}^2 + \sum_{E \in \mathcal{E}^0} h_E \|\{\{\nabla(p_h - \zeta)\}\}\|_{0,E}^2 + \sum_{E \in \mathcal{E}^0} h_E^{-1} \|\llbracket p_h \rrbracket\|_{0,E}^2 \\
& + \sum_{E \in \mathcal{E}^D} h_E \|\mathbf{n}_E \cdot \nabla(p_h - \zeta)\|_{0,E}^2 + \sum_{E \in \mathcal{E}^D} h_E^{-1} \|p_h\|_{0,E}^2.
\end{aligned} \tag{58}$$

The terms $\nabla(p_h - \zeta)$ in (58) is bounded by $\sum_{K \in \mathcal{T}_h} \|\nabla(p_h - \zeta)\|_{0,K}^2$ by using the trace and inverse inequalities. Further, the latter is bounded by $\sum_{E \in \mathcal{E}^0} h_E^{-1} \|\llbracket p_h \rrbracket\|_{0,E}^2 + \sum_{E \in \mathcal{E}^D} h_E^{-1} \|p_h\|_{0,E}^2$, in view of the estimate in [27, Thm. 2.1]. Likewise, the term $\sum_{K \in \mathcal{T}_h} \|p_h - \zeta\|_{0,K}^2$ is also bounded by

$$\sum_{E \in \mathcal{E}^0} h_E \|\llbracket p_h \rrbracket\|_{0,E}^2 + \sum_{E \in \mathcal{E}^D} h_E \|p_h\|_{0,E}^2.$$

Finally, combining the bounds in (56)-(58) with $\|\nabla e_p\|_{0,K} \leq \|e_p\|$ and $\alpha \|e_p\|_{0,K} \leq \|e_p\|$ provided that $\lambda_i, i = 1, \dots, 9$ are sufficiently small, the desired result (50a) is obtained.

The proof of (50b) is carried out in the similar way. \square

Combining Lemmas 4.1 and 4.2, we obtain the following reliability estimate:

Theorem 4.3 *Let (y, p, u) and (y_h, p_h, u_h) be the solutions of (7) and (25), respectively, and let the co-control σ and the discrete co-control σ_h be defined in (8) and (26), respectively. Assume that all the conditions in Lemma 4.1 hold. Then,*

$$\|u - u_h\|_{0,\Gamma_N} + \|\sigma - \sigma_h\|_{0,\Gamma_N} + \|y - y_h\| + \|p - p_h\| \leq C(\eta + \theta). \tag{59}$$

4.2 Efficiency of the error estimator

Here we provide a lower bound, up to data oscillations, for the discretization errors in terms of the error estimator as given in (30). We will show that the local error estimators can be bounded from above by the local constituents of the error and associated data oscillations. We use the same arguments as in [39, 27]. The element and edge bubble functions, denoted by b_K and b_E , respectively, are defined by

$$\|b_K\|_{\infty,K} = 1, \quad b_K \in H_0^1(K) \quad \text{and} \quad \|b_E\|_{\infty,E} = 1, \quad b_E \in H_0^1(\omega_E), \tag{60}$$

where ω_E is the union of the two elements that share it. We recall from [39] that there exist constants, depending on the shape regularity of the triangulation \mathcal{T}_h such that

$$\|v\|_{0,K}^2 \leq c_1 (v, vb_K)_{0,K}, \quad K \in \mathcal{T}_h, \tag{61a}$$

$$\|vb_K\|_{0,K} \leq c_2 \|v\|_{0,K}, \quad K \in \mathcal{T}_h, \tag{61b}$$

$$|vb_K|_{1,K} \leq c_3 h_K^{-1} \|v\|_{0,K}, \quad K \in \mathcal{T}_h, \tag{61c}$$

$$\|w\|_{0,E}^2 \leq c_4 (w, wb_E)_{0,E}, \quad E \in \mathcal{E}_h, \tag{61d}$$

$$\|wb_K\|_{0,E} \leq c_5 \|w\|_{0,E}, \quad E \in \mathcal{E}_h, \tag{61e}$$

$$\|wb_E\|_{0,\omega_E} \leq c_6 h_E^{1/2} \|w\|_{0,E}, \quad \omega_E = K \cup K^e, \quad E = K \cap K^e, \tag{61f}$$

$$|wb_E|_{1,\omega_E} \leq c_7 h_E^{-1/2} \|w\|_{0,E}, \quad \omega_E = K \cup K^e, \quad E = K \cap K^e, \quad (61g)$$

for any element $K \in \mathcal{T}_h$, edge $E \in \mathcal{E}_h$, and polynomials v and w defined on elements and edges, respectively.

In the following, for a set of elements S , we denote by $\|\cdot\|_S$ the local energy norm

$$\|v\|_S = \left(\sum_{K \in S} (\|\nabla v_h\|_{0,K}^2 + \alpha \|v\|_{0,K}^2) + \sum_{E \in \mathcal{E}_h^0 \cup \mathcal{E}_h^p \subset S} (h_E \|\{\{\nabla v\}\}\|_{0,E}^2 + \frac{\sigma_0}{h_E} \|\llbracket v_h \rrbracket\|_{0,E}^2) \right)^{1/2}.$$

Lemma 4.4 *Let (y, p, u) and (y_h, p_h, u_h) be the solutions of (7) and (25), respectively, and let the error estimators $\eta_{y,K}$, $\eta_{p,K}$ and the data oscillations $\theta_{y,K}$, $\theta_{p,K}$ be given by (32) and (36), respectively. Then, we have*

$$\eta_{y,K}^2 \leq C \left(\|\nabla(y - y_h)\|_K^2 + \theta_{y,K}^2 \right), \quad (62a)$$

$$\eta_{p,K}^2 \leq C \left(\|\nabla(p - p_h)\|_K^2 + \theta_{p,K}^2 + h_K^2 \|y - y_h\|_{0,K}^2 \right). \quad (62b)$$

Proof. We define the residual $R = f_h + \Delta y_h - \alpha_h y_h$, and set $W = h_K^2 R b_K$, where b_K is the bubble function $27\lambda_1\lambda_2\lambda_3$ expressed in terms of the barycentric coordinates λ_j , $j = 1, 2, 3$, of K . By the inequality (61a),

$$h_K^2 \|R\|_{0,K}^2 \leq c_1 (R, W)_{0,K} = c_1 \left((f + \Delta y_h - \alpha_h y_h, W)_{0,K} + (f_h - f, W)_{0,K} \right).$$

Since the exact solution satisfies $(f + \Delta y - \alpha y)|_K = 0$, we obtain, using integration by parts and addition and subtraction of the exact data, that

$$h_K^2 \|R\|_{0,K}^2 \leq c_1 \left((\nabla(y - y_h), \nabla W)_{0,K} + (f_h - f, W)_{0,K} + ((\alpha - \alpha_h)y_h, W)_{0,K} \right).$$

Here, we also used that $W|_{\partial\Omega} = 0$. By the inequalities (61b), (61c) and an application of Young's inequality, we obtain

$$h_K^2 \|R\|_{0,K}^2 \leq C \left(\|\nabla(y - y_h)\|_{0,K}^2 + h_K^2 \|f - f_h\|_{0,K}^2 + h_K^2 \|(\alpha - \alpha_h)y_h\|_{0,K}^2 \right) + C\delta \|R\|_{0,K}^2,$$

which is the desired result (62a) for sufficiently small δ . The inequality (62b) can be proven analogously. \square

Lemma 4.5 *Let (y, p, u) and (y_h, p_h, u_h) be the solutions of (7) and (25), respectively, and let the error estimators $\eta_{y,K}$, $\eta_{p,K}$ and the data oscillations $\theta_{y,K}$, $\theta_{p,K}$ be given by (32) and (36), respectively. In addition, let $\omega_E = K \cup K^e$ be the union of any two elements, i.e., K, K^e with $E = K \cap K^e$. Then, we have*

$$h_E \|\llbracket \nabla y_h \rrbracket\|_{0,E}^2 \leq C \left(\|y - y_h\|_{\omega_E}^2 + \sum_{K=K, K^e} \eta_{y,K}^2 + \sum_{K=K, K^e} \theta_{y,K}^2 \right), \quad (63a)$$

$$h_E \|\llbracket \nabla p_h \rrbracket\|_{0,E}^2 \leq C \left(\|p - p_h\|_{\omega_E}^2 + \sum_{K=K, K^e} \eta_{p,K}^2 + \sum_{K=K, K^e} \theta_{p,K}^2 \right). \quad (63b)$$

Proof. We set $W = \llbracket \nabla y_h \rrbracket b_E$, where b_E is the bubble edge function on ω_E given by

$$b_E|_K = 4\lambda_1\lambda_2, \quad b_E|_{K^e} = 4\lambda_1^e\lambda_2^e.$$

By using the inequality (61d) and the fact that $\llbracket \nabla y \rrbracket = 0$ on the interior edges, we obtain

$$h_E \|\llbracket \nabla y_h \rrbracket\|_{0,E}^2 \leq c_4 h_E (\llbracket \nabla y_h \rrbracket, W)_{0,E} = c_4 h_E (\llbracket \nabla (y_h - y) \rrbracket, W)_{0,E}.$$

After integration by parts over each of the two elements of $\omega_E = K \cup K^e$, we have

$$(\llbracket \nabla (y_h - y) \rrbracket, W)_{0,E} = (\Delta (y_h - y), w)_{0,\omega_E} + (\nabla (y_h - y), \nabla w)_{0,\omega_E}.$$

Using the differential equation $-\Delta y + \alpha y = f$ and approximating the data, we obtain

$$\begin{aligned} h_E \|\llbracket \nabla y_h \rrbracket\|_{0,E}^2 &\leq c_4 h_E \left((f_h + \Delta y_h - \alpha_h y_h, W)_{0,\omega_E} + (f - f_h, W)_{0,\omega_E} + ((\alpha_h - \alpha) y_h, W)_{0,\omega_E} \right) \\ &\quad + c_4 h_E \left((\alpha (y_h - y), W)_{0,\omega_E} + (\nabla (y_h - y), \nabla W)_{0,\omega_E} \right). \end{aligned}$$

Then, the inequalities (61f) and (61g) yield

$$h_E \|\llbracket \nabla y_h \rrbracket\|_{0,E}^2 \leq C h_E^{1/2} \|\llbracket \nabla y_h \rrbracket\|_{0,E} \left(\|y - y_h\|_{\omega_E} + \left(\sum_{K=K,K^e} \eta_{y,K}^2 \right)^{1/2} + \left(\sum_{K=K,K^e} \theta_{y,K}^2 \right)^{1/2} \right),$$

which gives the desired result (63a) after an application of Young's inequality and the shape-regularity of the mesh, i.e., $h_E \leq \gamma h_K$ with $\gamma > 1$. The proof of (63b) is carried out in the similar way. \square

Lemma 4.6 *Let (y, p, u) and (y_h, p_h, u_h) be the solutions of (7) and (25), respectively, and let η_{y,E^N} and η_{p,E^N} and the data oscillations $\theta_{y,K}, \theta_{y,E^N}, \theta_{p,K}$ be given by (34b) and (36), respectively. Then, we have*

$$\eta_{y,E^N}^2 \leq C \left(\|y - y_h\|_K^2 + \eta_{y,K}^2 + \theta_{y,K}^2 + \theta_{y,E^N}^2 + \|u - u_h\|_{0,E}^2 \right), \quad (64a)$$

$$\eta_{p,E^N}^2 \leq C \left(\|p - p_h\|_K^2 + \eta_{p,K}^2 + \theta_{p,K}^2 \right). \quad (64b)$$

Proof. We set $W = (\mathbf{n}_E \cdot \nabla y_h - u_h - g_h^N) b_E$, where b_E is the bubble edge function. By using the inequality (61d) and the fact that $\mathbf{n}_E \cdot \nabla y = u + g^N$ on the Neumann boundary edges, we obtain

$$\begin{aligned} \eta_{y,E^N}^2 &= h_E \|u_h + g_h^N - \mathbf{n}_E \cdot \nabla y_h\|_{0,E}^2 \\ &\leq c_4 h_E (\mathbf{n}_E \cdot \nabla y_h - u_h - g_h^N, W)_{0,E} \\ &= c_4 h_E \left((\mathbf{n}_E \cdot \nabla (y_h - y), W)_{0,E} + (u - u_h, W)_{0,E} + (g^N - g_h^N, W)_{0,E} \right). \end{aligned}$$

By integration by part over the element $K \supset E$, the differential equation $-\Delta y + \alpha y = f$ and approximating the data, we obtain

$$\begin{aligned} \eta_{y,E^N}^2 &\leq c_4 h_E \left((f_h + \Delta y_h - \alpha_h y_h, W)_{0,K} + (f - f_h, W)_{0,K} + ((\alpha_h - \alpha) y_h, W)_{0,K} \right) \\ &\quad + c_4 h_E \left((\alpha (y_h - y), W)_{0,K} + (\nabla (y_h - y), \nabla w)_{0,K} \right) \\ &\quad + c_4 h_E \left((u - u_h, W)_{0,E} + (g^N - g_h^N, W)_{0,E} \right). \end{aligned}$$

Then, the inequalities (61e)-(61g) yield

$$\eta_{y,E^N}^2 \leq Ch_E^{1/2} \|u_h + g_h^N - \mathbf{n}_E \cdot \nabla y_h\|_{0,E} \left(\|y - y_h\|_K + \eta_{y,K}^2 + \theta_{y,K}^2 + \theta_{y,E^N}^2 + \|u - u_h\|_{0,E}^2 \right).$$

Finally, by applying Young's inequality, we obtain the desired result (64a). The proof of (64b) can be verified by using the same arguments. \square

What is now left is to bound the estimator for the discretization error in the controls.

Lemma 4.7 *Let (y, p, u) and (y_h, p_h, u_h) be the solutions of (7) and (25), respectively, and let η_{u,E^N} and θ_u be given by (34c) and (36), respectively. Then, we have*

$$\begin{aligned} \eta_{u,E^N}^2 \leq & C \left(\|u - u_h\|_{0,\Gamma_N}^2 + \|p - p_h\|_K^2 + \theta_u^2 \right. \\ & \left. + h_E \|(\mathbf{n}_E \cdot \nabla(\omega(u_h - u_h^d) - p_h))\chi_{\mathcal{A}_h}\|_{0,E}^2 \right), \end{aligned} \quad (65)$$

where \mathcal{A}_h is the union of the active sets $\mathcal{A}_{a,h}$ and $\mathcal{A}_{b,h}$.

Proof. We have that $(\omega(u - u^d) - p)\chi_I = 0$ from (11). It follows from the inverse inequality (20) that

$$\begin{aligned} \eta_{u,E^N}^2 &= h_E \|\mathbf{n}_E \cdot \nabla(\omega(u_h - u_h^d) - p_h)\|_{0,E}^2 \\ &\leq C \|(\omega(u_h - u_h^d) - p_h)\chi_{I_h}\|_{0,E} + h_E \|(\mathbf{n}_E \cdot \nabla(\omega(u_h - u_h^d) - p_h))\chi_{\mathcal{A}_h}\|_{0,E}^2 \\ &= C \|(\omega(u_h - u_h^d) - p_h - \omega(u - u^d) + p)\chi_{I_h}\|_{0,E}^2 + h_E \|(\mathbf{n}_E \cdot \nabla(\omega(u_h - u_h^d) - p_h))\chi_{\mathcal{A}_h}\|_{0,E}^2 \\ &\leq C (\|u - u_h\|_{0,E}^2 + \|\omega(u - u^d) - p\|_{0,E}^2 + \|p - p_h\|_{0,E}^2) + h_E \|(\mathbf{n}_E \cdot \nabla(\omega(u_h - u_h^d) - p_h))\chi_{\mathcal{A}_h}\|_{0,E}^2. \end{aligned}$$

This is the desired inequality. \square

Now, we can derive the efficiency estimate in the following theorem.

Theorem 4.8 *Let (y, p, u) and (y_h, p_h, u_h) be the solutions of (7) and (25), respectively, and the error estimator η and data oscillation θ be given as in (31) and (35), respectively. Then, it holds*

$$\begin{aligned} \eta \leq & C \left(\|u - u_h\|_{0,\Gamma_N} + \|y - y_h\| + \|p - p_h\| + \theta \right. \\ & \left. + \sum_{E \in \mathcal{E}_h^N} h_E \|(\mathbf{n}_E \cdot \nabla(\omega(u_h - u_h^d) - p_h))\chi_{\mathcal{A}_h}\|_{0,E} \right). \end{aligned} \quad (66)$$

Proof. By the definition of the energy norm defined in (23), and the fact that $[[y]] = 0$ on the interior edges and $y = g^D$ on the Dirichlet boundary edges, we can easily derive

$$\sum_{E \in \mathcal{E}_h^0} \frac{\sigma_0^2}{h_E} \|[[y_h]]\|_{0,E}^2 + \sum_{E \in \mathcal{E}_h^D} \frac{\sigma_0^2}{h_E} \|g_h^D - y_h\|_{0,E}^2 \leq C (\|y - y_h\|^2 + \sum_{E \in \mathcal{E}_h^D} h_E^{-1} \|g^D - g_h^D\|_{0,E}^2). \quad (67)$$

Analogously, we obtain

$$\sum_{E \in \mathcal{E}_h^0} \frac{\sigma_0^2}{h_E} \|[[p_h]]\|_{0,E}^2 + \sum_{E \in \mathcal{E}_h^D} \frac{\sigma_0^2}{h_E} \|p_h\|_{0,E}^2 \leq C \|p - p_h\|^2. \quad (68)$$

Then, the combination of the results in Lemma 4.4-4.6 with the inequalities (67)-(68) gives the assertion (66). \square

Remark 4.9 *In our numerical experiments, we use*

$$\tilde{\eta}_u = \sum_{E \in \mathcal{E}_h^N} h_E \|(\mathbf{n}_E \cdot \nabla(\omega(u_h - u_h^d) - p_h))\chi_{I_h}\|_{0,E} \quad (69)$$

as an indicator of the control instead of η_u (31c), since η_u does not lead to a localization of refinement of the inactive set. The same problem is also observed for the control indicators proposed in [22, 28, 33].

In addition, we approximate the characteristic function by a posteriori quantities as done in [32]. For $\mu > 0$, let

$$\chi_{I_h} = \frac{(u_h - u_h^a)(u_h^b - u_h)}{h^\mu + (u_h - u_h^a)(u_h^b - u_h)}.$$

5 Implementation details

5.1 The adaptive loop

An adaptive procedure for the symmetric interior penalty Galerkin discretization of the optimization problem (2)-(3) consists of successive loops of the following sequence:

SOLVE \rightarrow **ESTIMATE** \rightarrow **MARK** \rightarrow **REFINE**.

The **SOLVE** step is the numerical solution of the optimal control problem with respect to the given triangulation \mathcal{T}_h using the SIPG discretization. By using the primal dual active set (PDAS) algorithm as a semi-smooth Newton step, see, e.g., [6], we solve the following discrete linear system:

$$\begin{pmatrix} \mathcal{M} & \cdot & \mathcal{K}^T & \cdot \\ \cdot & \omega\mathcal{M}_B & -\mathcal{M}_B & \mathcal{M}_B \\ \mathcal{K} & -\mathcal{M}_B & \cdot & \cdot \\ \cdot & \gamma\chi_{\mathcal{A}_h} & \cdot & \chi_{I_h} \end{pmatrix} \begin{pmatrix} y_h \\ u_h \\ p_h \\ \sigma_h \end{pmatrix} = \begin{pmatrix} \mathcal{M}y^d \\ \omega\mathcal{M}_B u^d \\ \mathcal{F} \\ \gamma(\chi_{\mathcal{A}_{a,h}} u^a + \chi_{\mathcal{A}_{b,h}} u^b) \end{pmatrix}, \quad (70)$$

where $\mathcal{A}_h = \mathcal{A}_{a,h} \cup \mathcal{A}_{b,h}$ is a diagonal 0-1-matrix. $\chi_{\mathcal{A}_{a,h}}$, $\chi_{\mathcal{A}_{b,h}}$ and $\chi_{\mathcal{A}_h}$ denote the characteristic functions of $\mathcal{A}_{a,h}$, $\mathcal{A}_{b,h}$ and \mathcal{A}_h , respectively. \mathcal{M} and \mathcal{M}_B are mass matrices on the domain and boundary, respectively. \mathcal{K} and \mathcal{F} correspond to the bilinear form $a_h(y_h, v_h)$ and the linear form $l_h(v_h)$ defined in (15), respectively.

For the **ESTIMATE** step, the residual error estimators η_y, η_p and η_u defined in Section 4 are used. In the **MARK** step of the adaptive loop, the edges and elements for the refinement are specified by using the a posteriori error estimator and by choosing subsets $\mathcal{M}_K \subset \mathcal{T}_h$ and $\mathcal{M}_E \subset \mathcal{E}_h$ such that the following bulk criterion [12] is satisfied for the given marking parameter Θ with $0 < \Theta < 1$:

$$\begin{aligned} \Theta \sum_{K \in \mathcal{T}_h} (\eta_K^y)^2 + (\eta_K^p)^2 &\leq \sum_{K \in \mathcal{M}_K} (\eta_K^y)^2 + (\eta_K^p)^2, \\ \Theta \sum_{E \in \mathcal{E}_h} (\eta_E^y)^2 + (\eta_E^p)^2 + (\eta_E^u)^2 &\leq \sum_{E \in \mathcal{M}_E} (\eta_E^y)^2 + (\eta_E^p)^2 + (\eta_E^u)^2. \end{aligned}$$

Bigger Θ will result in more refinement of triangles in one loop and smaller Θ will result in a more optimal grid but more refinement loops. We note that the data oscillations may be included in the bulk criterion in the same way. Finally, in the **REFINE** step, the marked elements are refined by longest edge bisection, whereas the elements of the marked edges are refined by bisection [9].

5.2 Numerical results

We now present several numerical results in order to examine the quality of the derived estimators in Section 4 and the performance of the adaptive loop introduced in Section 5.1. We use piecewise linear polynomials for the approximation of the state, the adjoint, the control and the co-control. The penalty parameter σ_0 in the SIPG is chosen as $\sigma_0 = 6$ on the interior edges and 12 on the boundary edges. The parameter γ used in the definition of the active and inactive sets is chosen as equal to the regularization parameter ω . The effective index is calculated according to

$$\text{effectivity index} = \frac{\eta_y + \eta_p + \eta_u}{\| \|y - y_h\| \| + \| \|p - p_h\| \| + \| \|u - u_h\| \|_{0,\Gamma_N} + \| \| \sigma - \sigma_h \| \|_{0,\Gamma_N}}. \quad (71)$$

We finally define the projection of the control such that

$$\text{Proj}_{u^a, u^b}(v) = \max\{u^a, \min\{u^b, v\}\}. \quad (72)$$

5.2.1 Example 1

We use an example on the L-shaped domain, which is given by as $\Omega = (-1, 1)^2 \setminus ([0, 1] \times (-1, 0])$ with $\Gamma = \Gamma_N$, see Figure 1. The control is defined all Neumann boundary. The box constraints are given by $u^a = -0.5$ and $u^b = 0.5$. The reaction term α and the regularization parameter ω are taken as $\alpha = 1$ and $\omega = 1$, respectively. The remaining data of the problem are

$$f(r, \theta) = 0, \quad u^d(r, \theta) = 0, \quad g^N(r, \theta) = -\text{Proj}_{u^a, u^b}(r^{2/3} \sin(\frac{2}{3}\theta)), \quad y^d(r, \theta) = r^{2/3} \sin(\frac{2}{3}\theta),$$

where $r = \sqrt{x_1^2 + x_2^2}$, $\forall (x_1, x_2) \in \Omega$ and $\theta = \begin{cases} \text{atan2}(x_1, x_2), & \text{atan2}(x_1, x_2) \geq 0, \\ \text{atan2}(x_1, x_2) + 2\pi, & \text{atan2}(x_1, x_2) < 0 \end{cases}$ with the function $\text{atan2}(x_1, x_2)$, i.e., four-quadrant inverse tangent (arctangent) of x_1 and x_2 . Note that the function $\text{atan2}(x_1, x_2)$ is defined in MATLAB[®].

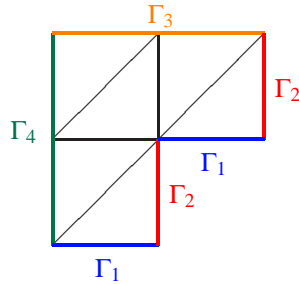


Figure 1: Example 5.2.1: L-shaped domain.

The analytical solutions of the state, adjoint, control and co-control are given by

$$\begin{aligned} y(r, \theta) &= 0, \\ p(r, \theta) &= r^{2/3} \sin\left(\frac{2}{3}\theta\right), \\ u(r, \theta) &= \text{Proj}_{u^a, u^b}\left(r^{2/3} \sin\left(\frac{2}{3}\theta\right)\right), \\ \sigma(r, \theta) &= r^{2/3} \sin\left(\frac{2}{3}\theta\right) - \text{Proj}_{u^a, u^b}\left(r^{2/3} \sin\left(\frac{2}{3}\theta\right)\right), \end{aligned}$$

respectively.

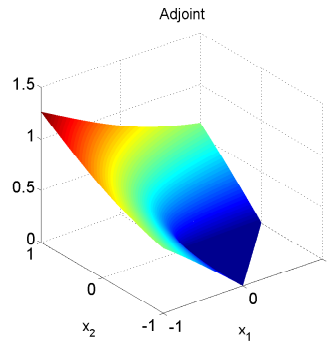


Figure 2: Example 5.2.1: Computed solution of the adjoint p .

The adjoint exhibits a typical singularity at the re-entrant corner of the domain Ω , see Figure 2. Figure 3 displays the computed control u and the computed co-control σ on the Neumann boundary. We observe that inactive set is equal to

$$I = [-0.78, 0] \times \{-1\} \cup [0, 1] \times \{0\} \cup \{0\} \times [-1, 0] \cup \{1\} \times [0, 0.78]. \quad (73)$$

The initial mesh is generated by starting first dividing Ω into uniform squares and then dividing each square into two triangles. It should be emphasized that we are working with a single mesh for all variables. Consequently, the mesh reflects regions of substantial change in the variables. Figure 4 shows the adaptively generated triangulations after seven refinement steps with $\Theta = 0.50$ in the bulk criteria. The more refinements occurs on the one hand for the singularity of the adjoint at the re-entrant corner, and on the other hand for the discretization of the control in the inactive set I (73), as we expected.

Figure 5 displays the performance of the error estimator proposed in Section 4 in terms of number of vertices for the marking parameter $\Theta = 0.5$. The left plot shows the effectivity index of the estimator, which is the ratio between the error measured in the $\|\cdot\|$ -norm and the estimator, defined in (71). Some minimal resolutions are necessary so that the ratio becomes constant.

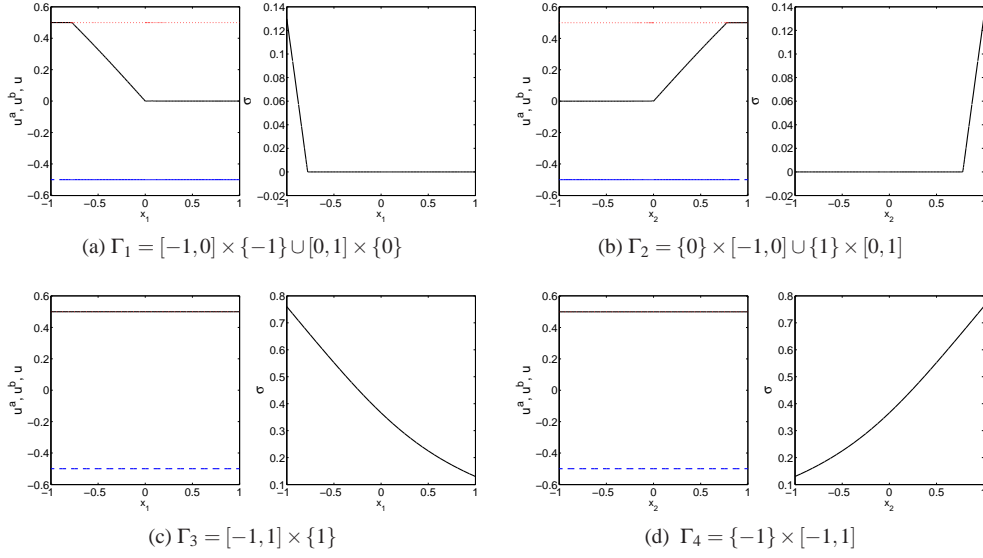


Figure 3: Example 5.2.1: The computed control u and the computed co-control σ on the Neumann boundary regions.

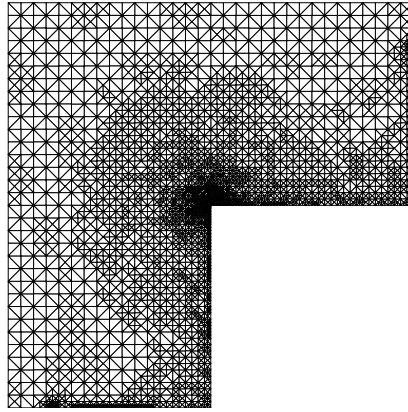


Figure 4: Example 5.2.1: Adaptively generated mesh after 7 refinement steps with $\Theta = 0.50$ in the bulk criteria.

The middle plot displays that the $\|\cdot\|$ -error and estimator η decay with a rate close to the optimal rate $N^{-1/2}$, where N is the number of vertices. Lastly, the right plot shows the actual size of the state, adjoint and control related components of the error estimator and data oscillation. As can be expected, the adjoint component of the estimator is dominant due to the singularity at the reentrant corner of Ω . Since the desired control u^d and the bounds of the control, i.e., u^a, u^b are constants, the data oscillation of the control θ_u is equal to zero.

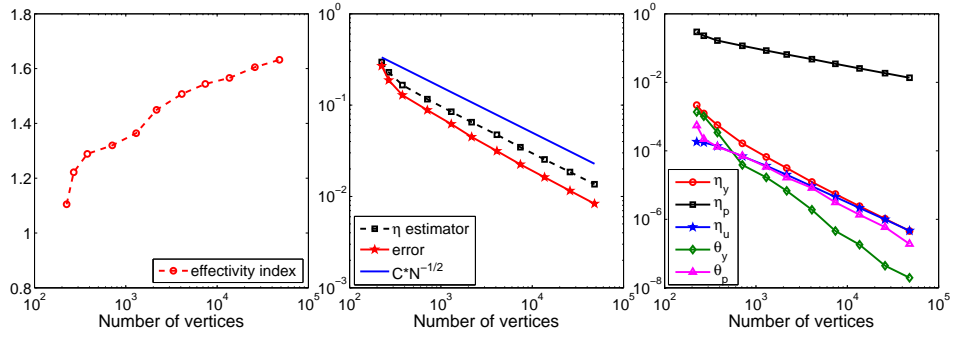


Figure 5: Example 5.2.1: The left plot shows the effectivity index. The middle plot shows the decay of the total error and estimator. The right plot shows the components of the error estimator and data oscillation. The marking parameter is $\Theta = 0.50$ in the bulk criteria.

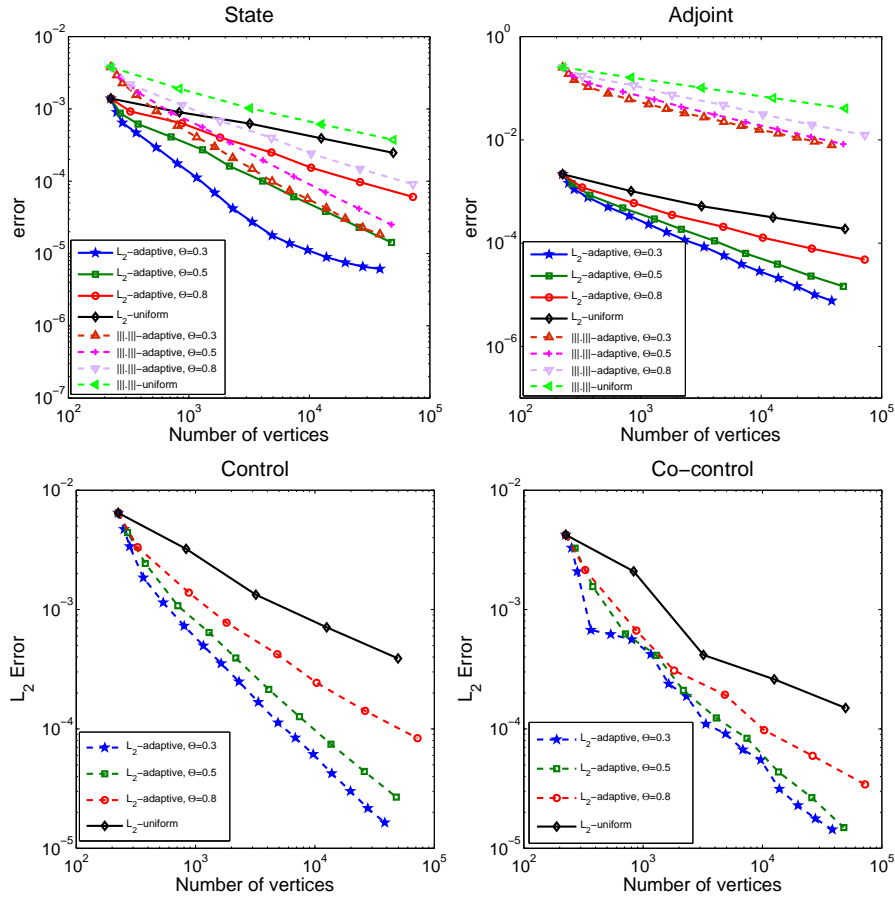


Figure 6: Example 5.2.1: The global errors of the state, adjoint in $\|\cdot\|$ and L^2 -norms (top), and of the control and co-control in L^2 -norm on adaptively and uniformly refined meshes with various marking parameters $\Theta = 0.3, 0.5, 0.8$ in the bulk criteria.

We next have a closer look the convergence of the state, adjoint, control and co-control variables. Figure 6 illustrates the errors of the state and adjoint in the $\|\cdot\|$ and L^2 -norms, and of the control and co-control in the L^2 -norm on adaptively and uniformly refined meshes with various marking parameters $\Theta = 0.3, 0.5, 0.8$. For all case, the adaptive refinements lead to better approximate solutions than the uniform refinements. Although the smaller Θ require more refinement loops, it produces more accurate results due to the obtained optimal mesh.

5.2.2 Example 2

This example is taken from [28]. Kohls et al. have solved this example by using a hierarchical estimator, discretized by a continuous finite element approximation. We let $\Omega = [0, 3]^2$ with $\Gamma = \Gamma_N$. However, the boundary control is only considered on $\{0\} \times [1, 2]$. The reaction term α and the regularization parameter ω are taken as $\alpha = 1$ and $\omega = 1$, respectively. The remaining setup of the problem is as follows:

$$\begin{aligned} f(x_1, x_2) &= e^{-10r^2} (41 - 400r^2), \\ u^d(x_1, x_2) &= 0, \\ g^N(x_1, x_2) &= \begin{cases} -\text{Proj}_{u^a, u^b} \left(\frac{Z}{2n} \left((2n+1) \left(\frac{2}{3}x_2 - 1 \right) - \left(\frac{2}{3}x_2 - 1 \right)^{2n+1} \right) \right), & (x_1, x_2) \in \{0\} \times [1, 2], \\ -60e^{-10(9+y^2)}, & x_1 = 3, \\ -60e^{-10(x^2+9)}, & x_2 = 3, \\ 0, & \text{otherwise,} \end{cases} \\ y^d(x_1, x_2) &= e^{-10r^2} + Z \left(\frac{2n+1}{2n} \left(\frac{2}{3}x_2 - 1 \right) + \frac{8n+4}{9} \left(\frac{2}{3}x_2 - 1 \right)^{2n-1} - \left(\frac{2}{3}x_2 - 1 \right)^{2n+1} \right), \end{aligned}$$

where $r = \sqrt{x_1^2 + x_2^2}$, $\forall (x_1, x_2) \in \Omega$. The analytical solutions of the state, adjoint, control and co-control are given by

$$\begin{aligned} y(r, \theta) &= e^{-10r^2}, \\ p(r, \theta) &= \frac{Z}{2n} \left((2n+1) \left(\frac{2}{3}x_2 - 1 \right) - \left(\frac{2}{3}x_2 - 1 \right)^{2n+1} \right), \\ u(r, \theta) &= \text{Proj}_{u^a, u^b} \left(\frac{Z}{2n} \left((2n+1) \left(\frac{2}{3}x_2 - 1 \right) - \left(\frac{2}{3}x_2 - 1 \right)^{2n+1} \right) \right), \\ \sigma(r, \theta) &= \frac{Z}{2n} \left((2n+1) \left(\frac{2}{3}x_2 - 1 \right) - \left(\frac{2}{3}x_2 - 1 \right)^{2n+1} \right) \\ &\quad - \text{Proj}_{u^a, u^b} \left(\frac{Z}{2n} \left((2n+1) \left(\frac{2}{3}x_2 - 1 \right) - \left(\frac{2}{3}x_2 - 1 \right)^{2n+1} \right) \right), \end{aligned}$$

respectively, with $Z = 10, n = 20$. The components of the error estimator exhibit local refinements in different regions of the domain due to the particular features of the state, the adjoint, and the control. The state y needs more refinement around the origin due to the shape of the narrow exponential peak. The adjoint p displays a boundary layer close to $x_2 = 0$ and $x_2 = 3$. These features can be observed in Figure 7.

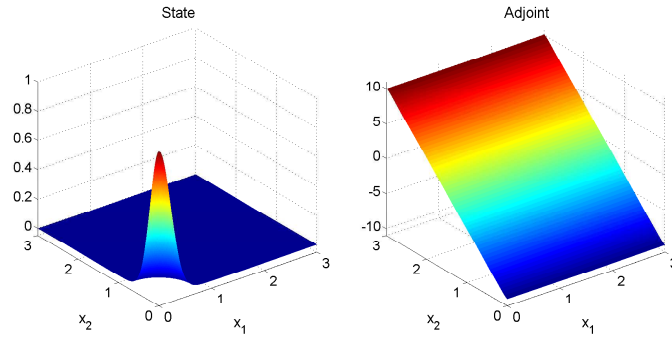


Figure 7: Example 5.2.2: Computed solutions of the state y (left) and the adjoint (right).

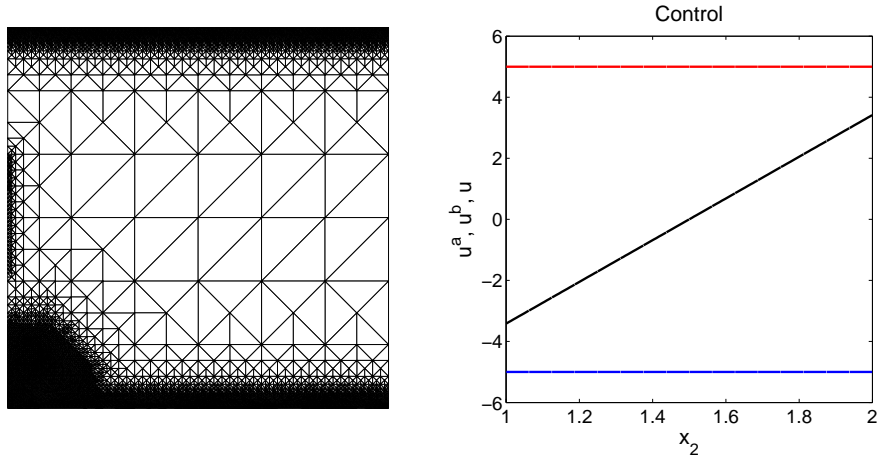


Figure 8: Example 5.2.2: Adaptively generated mesh (left) after 13 adaptive refinement step with $\Theta = 0.5$, and the computed control u (right) for the inactive case.

To observe the sensitivity of the adaptive algorithm with respect to the changes of the active and inactive sets, we test the example with different box constraints:

Inactive case: We first consider the control constraints as

$$u^a = -5 \quad \text{and} \quad u^b = 5.$$

Figure 8 reveals the adaptively refined mesh (left) and the computed control (right) for the inactive case. We observe that the control is between the lower bound and upper bound, i.e., $u^a < u < u^b$. Therefore, the inactive set I is equal to all of the control boundary, i.e.,

$I = \{0\} \times [1, 2]$. In the adaptive refinement, our error indicator $\tilde{\eta}_u$ (69) catches the inactive set well, see Figure 8 (left), after 13 adaptive refinement steps with $\Theta = 0.5$ in the bulk criteria. Further, the resolution of the state and the adjoint occur as expected.

Mixed case I: The control constraints are now considered as

$$u^a = -2 \quad \text{and} \quad u^b = 0.$$

Now, the value of control varies between the lower bound and upper bound:

$$u = u^a \quad \text{for } x_2 \in [1, 1.2] \quad \text{and} \quad u = u^b \quad \text{for } x_2 \in [1.4, 2].$$

Therefore, the inactive set $I = \{0\} \times [1.2, 1.4]$. Figure 9 reveals that the inactive set of the mixed case I are picked out well in the adaptive refinement.

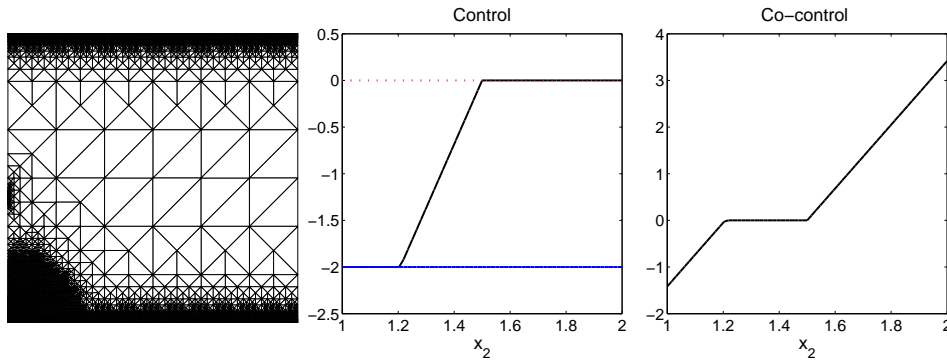


Figure 9: Example 5.2.2: Adaptively generated mesh (left) after 13 adaptive refinement step with $\Theta = 0.5$, and the computed control u (middle) and co-control σ (right) for the mixed case I.

Mixed case II: We finally considered the control constraints as

$$u^a = 0 \quad \text{and} \quad u^b = 2.$$

Now, the value of control varies between the lower bound and upper bound as the previous case:

$$u = u^a \quad \text{for } x_2 \in [1, 1.5] \quad \text{and} \quad u = u^b \quad \text{for } x_2 \in [1.8, 2].$$

Therefore, the inactive set $I = \{0\} \times [1.5, 1.8]$. As previous cases, the inactive set of the mixed case II are picked out well in the adaptive refinement, see Figure 10 (left).

We next have a closer look some properties of the proposed estimator for the inactive case. Figure 11 (left) displays the ratio between the error with $\|\cdot\|$ -norm and the estimator, called the effectivity index for the inactive case with the marking parameter $\Theta = 0.50$. The ratio converges to a constant after a few iterations.

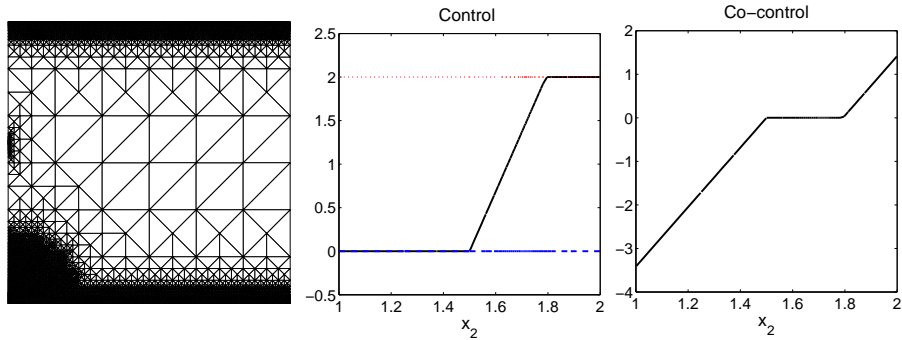


Figure 10: Example 5.2.2: Adaptively generated mesh (left) after 13 adaptive refinement step with $\Theta = 0.5$, and the computed control u (middle) and co-control σ (right) for the mixed case II.

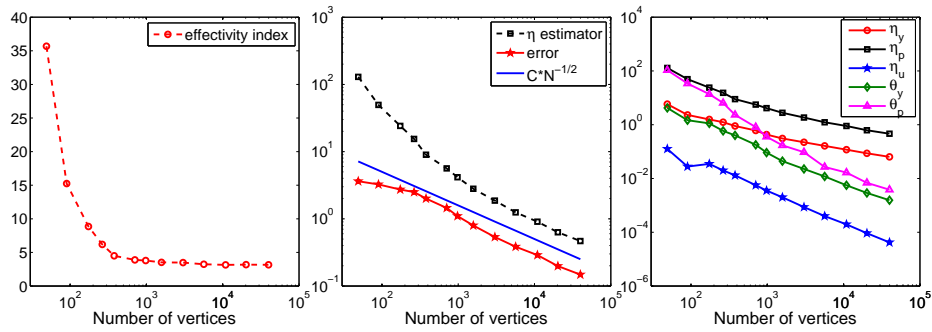


Figure 11: Example 5.2.2: The left plot shows the effectivity index. The middle plot shows the decay of the total error and estimator. The right plot shows the components of the error estimator and the data oscillation. The results are obtained for the inactive case with $\Theta = 0.50$ in the bulk criteria.

The middle plot in Figure 11 shows the decay of the error and estimator versus the number of vertices for the adaptive refinement. The estimator underestimates the error by an almost constant factor. We observe that the behaviour of the error and the estimator is similar to the results obtained in [28]. The right plot in Figure 11 shows the actual size of the state, adjoint and control related components of the error estimator and the data oscillations for the inactive case. The refinement process is dominated by the contribution of the adjoint.

Figure 12 finally illustrates the errors of the state and adjoint in the $\|\cdot\|$ and L^2 -norms, and of the control in the L^2 -norm on adaptively and uniformly refined meshes with various marking parameters $\Theta = 0.3, 0.5, 0.8$. The adaptive refinements lead to better approximate solutions than uniform refinements.

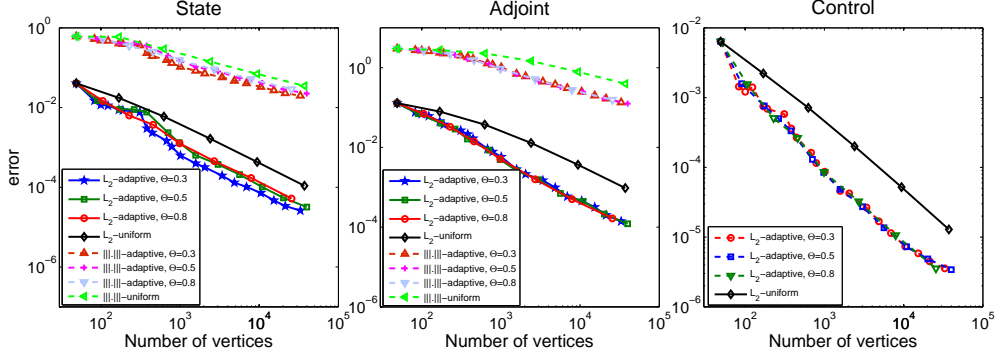


Figure 12: Example 5.2.2: Errors of the state y (left) and adjoint p (middle) in $\|\cdot\|$ and L^2 -norms, and the control u (right) in L^2 -norm on adaptively and uniformly refined meshes for the inactive case with various marking parameters $\Theta = 0.3, 0.5, 0.8$ in the bulk criteria.

5.2.3 Example 3

We use the example considered in [15]. Gaevskaya et al. have solved this example by using a residual-type error estimator, discretized by a continuous finite element approximation. In this example we use non-constant lower and upper bounds for the control, which are highly oscillating constraints. The data of the problem are

$$\Omega = (0, 1)^2, \quad \Gamma_N = (0, 1) \times \{0\}, \quad \Gamma_D = \partial \setminus \Gamma_N, \quad \alpha(x_1, x_2) = 1, \quad \omega = 10^{-3}, \quad u^d(x_1, x_2) = 0,$$

$$y^d(x_1, x_2) = \begin{cases} 0, & x_1 \leq 0.5, \\ 1, & 0.5 < x_1 < 0.75, \\ -1, & 0.75 < x_1, \end{cases}, \quad f(x_1, x_2) = 0, \quad g^D(x_1, x_2) = 0, \quad g^N(x_1, x_2) = 0,$$

$$u^a = \sin(8\pi x_1), \quad u^b = 2 + \cos(\pi/2 + 8x_1).$$

Figures 13 and 14 show the computed solutions of the state y , the adjoint p , the control u , and the co-control σ , respectively. The control switches from the lower to the upper bound and back again to the lower bound on Γ_N . This is an almost "bang-bang" type optimal control.

The initial mesh is generated by starting first dividing Ω into 8×8 uniform squares and then dividing each square into two triangles as in the previous examples. Adaptively generated meshes after six (left) and eight (right) refinements are displayed in Figure 15 with $\Theta = 0.45$ in the bulk criterion. As expected, more refinements occur on the one hand for the discretization of the control in the inactive set, almost Neumann boundary Γ_N , and on the other hand for the discretization of the state and adjoint on the right side of the mesh, i.e., $(0.5, 1) \times (0, 1)$.

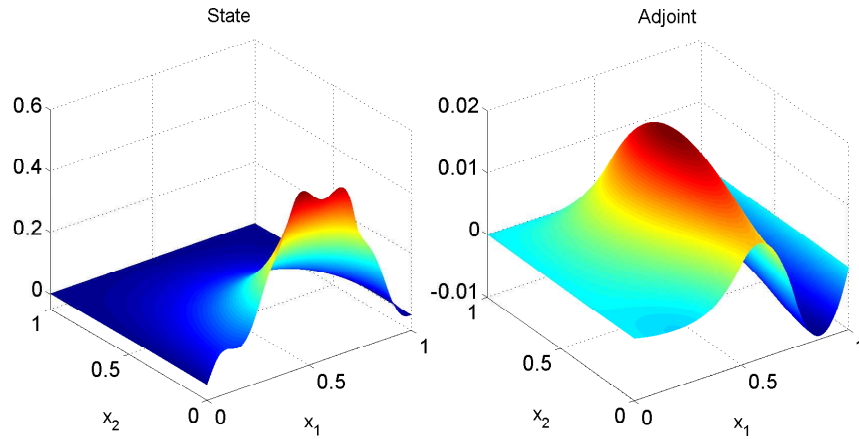


Figure 13: Example 5.2.3: Computed solutions of the state y (left) and of the adjoint p (right).

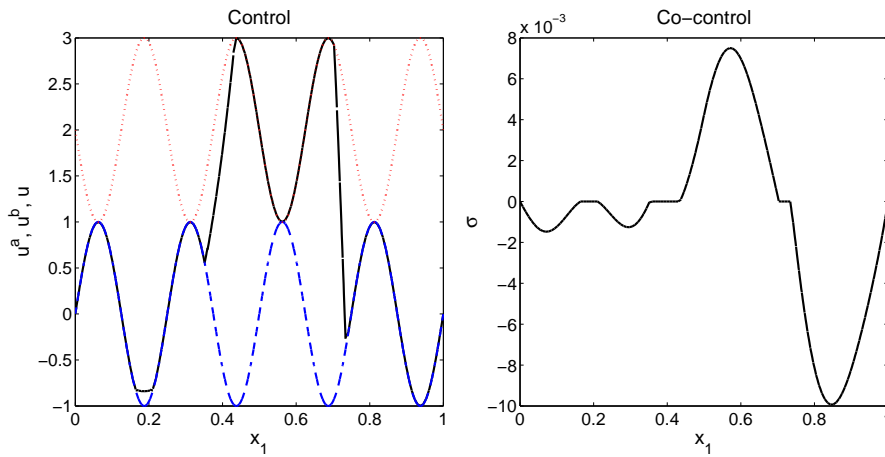


Figure 14: Example 5.2.3: Computed solutions of the control u (left) and of the co-control σ (right). The lower and upper bounds on the control, i.e., u^a and u^b , are shown as 'dashed (blue)' and 'dotted (red)' lines, respectively.

The components of the residual type a posteriori error estimator and data oscillations are presented in Table 1 on the mesh hierarchy with $\Theta = 0.45$ in the bulk criterion. We observe that dominating contributions such as the state estimator η_y , the adjoint estimator η_p , and the control oscillation θ_u are smaller than obtained in [15] for approximately the same number of vertices.

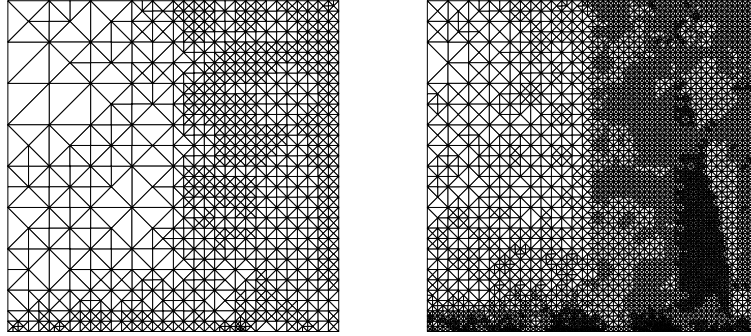


Figure 15: Example 5.2.3: Adaptively generated meshes after 6 (left) and 8 (right) refinement steps with $\Theta = 0.45$ in the bulk criteria.

# vertices	η_y	η_p	η_u	θ_p	θ_u
81	4.83e-01	1.20e-01	5.30e-06	8.07e-02	1.00e+00
167	3.70e-01	8.03e-02	2.84e-06	3.93e-02	6.35e-01
332	2.80e-01	5.81e-02	9.21e-07	2.37e-02	3.89e-01
582	2.49e-01	4.42e-02	5.52e-07	1.39e-02	1.37e-01
1174	1.83e-01	3.26e-02	2.60e-07	9.51e-03	7.30e-02
2116	1.32e-01	2.46e-02	1.23e-07	6.02e-03	3.91e-02
4055	9.57e-02	1.90e-02	5.96e-08	3.80e-03	1.75e-02
7234	6.92e-02	1.44e-02	2.97e-08	2.11e-03	9.76e-03

Table 1: Example 5.2.3: Components of the error estimator and data oscillation for $\Theta = 0.45$.

6 Conclusions

In this paper, we study a posteriori error analysis of the symmetric interior penalty Galerkin (SIPG) method for the boundary optimal control problems governed by the elliptic PDEs with bilateral control constraints. Piecewise linear polynomials are used to discretize the unknown variables. The lower and upper error estimates are derived to show the efficiency and reliability of the proposed error estimator by invoking data oscillations. The numerical results show that the adaptive refinements are superior to uniform refinements. Future work will include the extension of our results to Dirichlet boundary optimal control problems.

Acknowledgements

This work was supported by the Forschungszentrum Dynamische Systeme (CDS): Biosystemtechnik, Otto-von-Guericke-Universität Magdeburg. Authors would like to thank Martin Stoll for helpful discussions about this research.

References

- [1] R.A. Adams. *Sobolev Spaces*. Academic Press, Orlando, San Diego, New-York, 1975.
- [2] M. Ainsworth. A posteriori error estimation for discontinuous Galerkin finite element approximation. *SIAM J. Numer. Anal.*, 45(4):1777–1798, 2007.
- [3] D. N. Arnold, F. Brezzi, B. Cockburn, and L. D. Marini. Unified analysis of discontinuous Galerkin methods for elliptic problems. *SIAM J. Numer. Anal.*, 39(5):1749–1779, 2002.
- [4] G. A. Baker, W. N. Jureidini, and O. A. Karakashian. Piecewise solenoidal vector fields and Stokes problem. *SIAM J. Numer. Anal.*, 27:1466–1485, 1990.
- [5] O. Benedix and B. Vexler. A posteriori error estimation and adaptivity for elliptic optimal control problems with state constraints. *Comput. Optim. App.*, 44(1):3–25, 2009.
- [6] M. Bergounioux, K. Ito, and K. Kunisch. Primal-dual strategy for constrained optimal control problems. *SIAM J. Control Optim.*, 37(4):1176–1194, 1999.
- [7] S. C. Brenner and L. R. Scott. *The Mathematical Theory of Finite Element Methods*. Springer Verlag, Berlin, Heidelberg, New York, second edition, 2002.
- [8] A. Cangiani, J. Chapman, E. H. Georgoulis, and M. Jensen. On local super-penalization of interior penalty discontinuous Galerkin methods. *Int. J. Numer. Anal. Mod.*, 11(3):478–495, 2014.
- [9] L. Chen. iFEM: an innovative finite element methods package in MATLAB. Technical report, Department of Mathematics, University of California, Irvine, CA 92697-3875, 2008.
- [10] D. Clever, J. Lang, S. Ulbrich, and J. C. Ziemis. Combination of an adaptive multi-level SQP method and a space-time adaptive PDAE solver for optimal control problems. *Procedia Computer Science*, 1(1):1435–1443, 2010.
- [11] L. Dedè, S. Micheletti, and S. Perotto. Anisotropic error control for environmental applications. *Appl. Numer. Math.*, 58(9):1320–1339, 2008.
- [12] W. Dörfler. A convergent adaptive algorithm for Poisson’s equation. *SIAM J. Numer. Anal.*, 33:1106–1124, 1996.
- [13] H. O Fattorini. *Infinite dimensional optimization and optimal control*. Encyclopedia of Mathematics, Vol. 62. Cambridge University Press, Cambridge, New York, 1999.
- [14] H. J. S. Fernando, S. M. Lee, and J. Anderson. Urban fluid mechanics: Air circulation and contaminant dispersion in cities. *Environmental Fluid Mechanics*, 1:107–164, 2001.
- [15] A. Gaevskaya, R. H. W. Hoppe, Y. Iliash, and M. Kieweg. A posteriori error analysis of control constrained distributed and boundary control problems. In *Proc. Conf. Scientific Computing*. Russian Academy of Sciences, Moscow, 2006.

- [16] A. Günther and M. Hinze. A posteriori error control of a state constrained elliptic control problem. *J. Numer. Math.*, 16:307–322, 2008.
- [17] J. S. Hesthaven and T. Warburton. *Nodal Discontinuous Galerkin Methods: Analysis, Algorithms, and Applications*. Springer-Verlag, Berlin, 2008.
- [18] M. Hintermüller and R. H. W. Hoppe. Goal-oriented adaptivity in pointwise state constrained optimal control of partial differential equations. *SIAM J. Control Optim.*, 48:5468–5487, 2010.
- [19] M. Hintermüller, R. H. W. Hoppe, Y. Iliash, and M. Kieweg. An a posteriori error analysis of adaptive finite element methods for distributed elliptic control problems with control constraints. *ESAIM Control Optim. Calc. Var.*, 14(3):540–560, 2008.
- [20] M. Hintermüller, K. Ito, and K. Kunisch. The primal-dual active set strategy as a semismooth Newton method. *SIAM J. Optim.*, 13(3):865–888, 2002.
- [21] M. Hinze, N. Yan, and Z. Zhou. Variational discretization for optimal control governed by convection dominated diffusion equations. *J. Comp. Math.*, 27(2-3):237–253, 2009.
- [22] R. H. W. Hoppe, Y. Iliash, C. Iyyunni, and N. H. Sweilam. A posteriori error estimates for adaptive finite element discretizations of boundary control problems. *J. Numer. Math.*, 14(1):57–82, 2006.
- [23] R. H. W. Hoppe, G. Kanschat, and T. Warburton. Convergence analysis of an adaptive interior penalty discontinuous Galerkin method. *SIAM J. Numer. Anal.*, 47(1):534–550, 2008/09.
- [24] R. H. W. Hoppe and M. Kieweg. Adaptive finite element methods for mixed control-state constrained optimal control problems for elliptic boundary value problems. *Comput. Optim. Appl.*, 46(3):511–533, 2010.
- [25] G. Kanschat. *Discontinuous Galerkin Methods for Viscous Incompressible Flow*. Advances in Numerical Mathematics. B. G. Teubner, Wiesbaden, 2007.
- [26] O. A. Karakashian and F. Pascal. A posteriori error estimates for a discontinuous Galerkin approximation of second-order elliptic problems. *SIAM J. Numer. Anal.*, 41(2):2374–2399, 2003.
- [27] O. A. Karakashian and F. Pascal. Convergence of adaptive discontinuous Galerkin approximations of second-order elliptic problems. *SIAM J. Numer. Anal.*, 45(2):641–665, 2007.
- [28] K. Kohls, A. Rösch, and K. Siebert. A posteriori error analysis of optimal control problems with control constraints. *SIAM J. Control. Optim.*, 52(3):1832–1861, 2014.
- [29] D. Leykekhman and M. Heinkenschloss. Local error analysis of discontinuous Galerkin methods for advection-dominated elliptic linear-quadratic optimal control problems. *SIAM J. Numer. Anal.*, 50(4):2012–2038, 2012.

- [30] R. Li, W. Liu, H. Ma, and T. Tang. Adaptive finite element approximation for distributed elliptic optimal control problems. *SIAM J. Control Optim.*, 41(5):1321–1349, 2002.
- [31] J.-L. Lions. *Optimal Control of Systems Governed by Partial Differential Equations*. Springer Verlag, Berlin, Heidelberg, New York, 1971.
- [32] W. Liu and N. Yan. A posteriori error estimators for a class of variational inequalities. *J. Sci. Comput.*, 35:361–393, 2000.
- [33] W. Liu and N. Yan. A posteriori error estimates for convex boundary control problems. *SIAM J. Numer. Anal.*, 39:73–99, 2001.
- [34] W. Liu and N. Yan. Local a posteriori error estimates for convex boundary control problems. *SIAM J. Numer. Anal.*, 47:1886–1908, 2009.
- [35] B. Mohammadi and O. Pironneau. *Applied Shape Optimization for Fluids*. Oxford University Press, Oxford, 2001.
- [36] P. Morin, R. H. Nochetto, and K. G. Siebert. Data oscillations and convergence of adaptive fem. *SIAM J. Numer. Anal.*, 38(2):466–488, 2000.
- [37] D. Parra-Guevara and Y. N. Skiba. On optimal solution of an inverse air pollution problem: theory and numerical approach. *Math. Comput. Modelling*, 43(7-8):766–778, 2006.
- [38] B. Rivière. *Discontinuous Galerkin methods for solving elliptic and parabolic equations. Theory and implementation*, volume 35 of *Frontiers in Applied Mathematics*. Society for Industrial and Applied Mathematics (SIAM), Philadelphia, PA, 2008.
- [39] R. Verfürth. *A Review of A Posteriori Error Estimation and Adaptive Mesh–Refinement Techniques*. Wiley-Teubner Series: Advances in Numerical Mathematics. Wiley Teubner, Chicester, New York, Stuttgart, 1996.
- [40] W. Wollner. A posteriori error estimates for a finite element discretization of interior point methods for an elliptic optimization problem with state constraints. *Comput. Optim. Appl.*, 47(1):133–159, 2010.
- [41] N. Yan and Z. Zhou. A priori and a posteriori error analysis of edge stabilization Galerkin method for the optimal control problem governed by convection-dominated diffusion equation. *J. Comput. Appl. Math.*, 223(1):198–217, 2009.
- [42] H. Yücel and P. Benner. Adaptive discontinuous Galerkin methods for state constrained optimal control problems governed by convection diffusion equations. *Comput. Optim. Appl.*, 2014. DOI:10.1007/s10589-014-9691-7.
- [43] H. Yücel, M. Heinkenschloss, and B. Karasözen. Distributed optimal control of diffusion-convection-reaction equations using discontinuous Galerkin methods. In *Numerical Mathematics and Advanced Applications 2011*, pages 389–397. Springer-Verlag Berlin Heidelberg, 2013.

- [44] H. Yücel and B. Karasözen. Adaptive symmetric interior penalty Galerkin (SIPG) method for optimal control of convection diffusion equations with control constraints. *Optimization*, 63:145–166, 2014.
- [45] Z. Zhou, X. Yu, and N. Yan. The local discontinuous Galerkin approximation of convection-dominated diffusion optimal control problems with control constraints. *Numer. Methods. Partial. Differ. Equ.*, 30(1):339–360, 2014.

